University of Natural Resources and Applied Life Sciences, Vienna
Institute of Surveying, Remote Sensing and Land Information

Master's Thesis

Estimation of Crop Water Requirements based on Remote Sensing Data

A Case Study of the Marchfeld Region in 2010

Author:
Nikolaus
NEUGEBAUER
Bakk. techn.

Supervisor:
Dr. Francesco
VUOLO

December 17, 2013

Contents

Chapter 1

Introduction

Even tough Marchfeld is one of the driest regions in Austria it is of high importance for the country's agricultural sector [1]. The low amount of precipitation in this part of Austria is overcome by irrigation systems. This artificial water supply does not only facilitate agricultural production itself but furthermore allows for high yield stability and crop quality, adding to the agricultural importance of the area. Especially in water-scarce regions the management of water resources is a delicate topic in need of precise monitoring and management. For the Marchfeld region, with agriculture being the main user of water, this means to estimate the need of water supply for crops to sustain optimal yield conditions. Efficient water management can not only help to reduce resource consumption but also to impede elution of nitrate which further improves water quality of the general area.

The maintenance of favourable yield conditions is the fundamental concept of agricultural production. Throughout history different kinds of techniques have been developed regarding to their cultural and environmental conditions. Domestication of plant and animal species as well as altering of soil, tillage, were among the first developments. Maintenance of soil fertility, control of pests and environmental conditions require advanced technologies, all of which aim to maintain or increase the output of agricultural production.

Early human civilizations had few possibilities to influence environmental conditions. One of them was and still is to overcome lacking amounts of precipitation by applying water to land in an artificial way. The earliest records of irrigation systems align with the spread of agricultural technology itself. The Sumerian culture developed methods to cultivate barley in an area with insufficient rainfall as early as the 6th millennium B.C.. Methods of flooding irrigation were used in Ancient Egypt, civilizations in India, Syria, China and America developed conceptual similar terrace irrigation. Records of canal irrigation technologies date back to 5th millennium B.C. [2].

Agriculture advanced with human civilizations, or vice versa. As with other technologies great advancements were achieved during the last century. Mechanization started to replace human labour, constraints of soil fertility were overcome by chemical fertilization and breeding of plant species developed further. All of these technologies are important contribution to today's agricultural systems. These technologies enabled high productivity of agriculture in various types of environments, ensuring food variety and security. The downside is that, without proper management, these techniques also start to effect the surrounding environment in a much larger scale [3]. Predicted future development of human population and current environmental degradation call for an intensification of agricultural production within given limitation of its surroundings. This means a form of "sustainable intensification" has to be achieved. As expressed by Mueller et al. [4] the necessity is to "*increase yields on under performing landscapes while simultaneously decrease[ing] the environmental impacts of agricultural systems* [5].

Advanced (sprinkler) irrigation systems have been introduced towards the end of the nineteenth century. This lead to both, an increase of agricultural production capacity and to challenges in rural water management. Irrigated agricultural surfaces produce 30 to 50% of the world's food crop on 17% of all arable land [6]. These numbers emphasize the high productive capacity of artificially irrigated agriculture. Overall 70% of freshwater withdraws are done by agricultural irrigation systems. The last decades saw a growth in the use of water resources which is predicted to further increase [7]. Water for agricultural irrigation is often pumped from ground water storages which has a large effect on the respective water bodies. The discharge from certain areas can lower groundwater levels on a large scale. Observation of the ground water development in the Middle East resulted in an estimated loss of ground water volumes of 144 cubic kilometres, equivalent to the amount of water stored in the Dead Sea, within the time period from 2003 to 2009. Although the influence of agricultural irrigation systems in these relations is not given, most of the discharge is an effect of reduced water supply during droughts, a time when water users turn to groundwater supplies [8]. Secondary problems are limited water supply for downstream users, water pollution, soil erosion and nutrient elution. Seepage losses of an inefficient irrigation system can accumulate in underlying groundwater, leading to water logging or salinity problems due to a rise of groundwater levels [9]. For some areas (like the one presented in this thesis) future development of climate is expected to result in a decline of precipitation rates and an increased likelihood of drought events [10, 11, 12, 13, 14].

As suggested by the European Environment Agency the improvement of irrigation systems, establishment of farmer advisory services and policy measures are tools to achieve a more sustainable use of water resources within the agricultural sector. Adjacent to nutrient management, efficient water management is considered to be the main component that can contribute to production increases (45% to 70% for most crops) thus supplying future food security in a sustainable way [4]. The increase in food demand is linked to the increase of human population. Recent decades brought a tremendous growth of human population from 2.5 billion in the 1950s to about 7.1 billion early 2013. Regarding food supply and food production the aim is to increase water productivity rather than reduce the general amount of water used ("more crop per drop") [15, 16]. Efficient irrigation management can also help to reduce the expansion of farmland. This is required for the upkeep of increasing agricultural production for food supply and security under limiting spatial conditions (competing non-agricultural land-uses). These developments can be supported by providing reliable and accurate information of crop water requirements to managers and farmers running agricultural irrigation systems.

Much development has been made in the way water is conveyed from water sources to fields. Increases in the efficiency of agricultural production were achieved by building new water ways (like the Marchfeldkanal) and developing technologies for the actual application of water to fields, like sprinkler irrigation systems. To achieve further efficiency in water use the question of water application at field level has to be addressed. This means an estimation of the amount of water needed by a given crop has to be performed with precise information about the temporal (when?) and spatial (where?) aspect.

To achieve this goal accurate information about the observed agricultural system is needed. Due to the nature of agricultural production the productivity depends highly on spatial and temporal factors. A seasonal (temporal) aspect is introduced by vegetation dynamics over the four seasons. Spatial variation is related to climatic conditions on large scale, and on smaller scale related to other factors like land use, management practices, soil type, fertility, etc.

Information regarding above mentioned characteristics can be obtained by using Remote Sensing (RS), and more specific, Earth Observation (EO) technologies. It provides the ability to acquire information of large areas with relatively short time intervals. Remote Sensing refers to the acquisition of information of an object or a phenomenon with no direct physical contact to it. Although remote sensing is mainly associated with interpretation of optical imagery

from satellite or aircraft there are many different platforms and applications in different fields like industrial quality control, security surveillance, medical applications and monitoring of hazardous environments and/or -objects. Amongst the first applications of remote sensing was the mapping of the land surface, photogrammetry and photo interpretation. The study of plant dynamics using this technology was introduced by Robert Colwell in the 1950s who used aerial colour-infrared photography to identify cereal crop, diseases and other problems in plant sciences [17].

The development of satellite- and digital technology later on brought the possibility of satellite based Remote Sensing. First photographs of the earth's surface from space were done by the Mercury-Mission in 1965. One year later, 1966, the "Earth Resources Technology Satellite Program" was initiated. The name of the program was later changed to "Landsat" (1975) and is still continued to this date with the last satellite launch (Landsat Data Continuity Mission, Landsat 8) on February 11, 2013. Since then satellites provided large amounts of data for the study of vegetation dynamics.

The fundamental concept of the study of vegetation dynamics through remote sensing systems is to derive characteristics of plants through their reflectance of radiation towards the sensor. A lot of information about the plant-canopy can be obtained by the relation of red to near-infra-red reflectance, therefore data for the study of vegetation is mainly acquired by multi-spectral, optical sensors. Information recorded by these sensors can be used to determine vegetation indices (VI) by few spectral bands only or used for a deduction of biochemical or biophysical characteristics through higher spectral resolution (empirically or physically based methods).

Biochemical and biophysical parameters like the the Leaf Area Index (LAI, one sided surface area of green leaves per ground surface area) are a common source of information for the study of vegetation status and dynamics and the application of remote sensing in agriculture technologies. These parameters can be derived from VIs which are calculated from measurements in two (or more) spectral bands [18]. The majority of VIs is derived from the relation of red- to near-infra-red reflectance. For vegetated surfaces this region exhibits a large increase of reflectance. This difference represents a basic VI, where the radiation reflected in near-infra-red is subtracted by the radiation reflected in red (*Difference vegetation index*; $DVI = \rho_{NIR} - \rho_R$). A normalisation of this index can be achieved by dividing the sum of near infra-red and red reflectance leading to the "*normalized difference vegetation index*"; $NDVI = (\rho_{NIR} - \rho_R)/(\rho_{NIR} + \rho_R)$. The normalisation helps to eliminate influence of different illumination and serves for better comparability. A list of vegetation indices (VIs) is given by Jones et al.[18] Vegetation indices help to identify a relation from spectral reflectance to actual variables of the observed canopy such as biomass, chlorophyll content or Leaf Area Index.

Leaf Area Index (LAI) is a key parameter to monitor vegetation dynamics. It is defined as the total one sided area of green leaf per unit ground surface area [19]. LAI is used to derive agronomical indicators for various crop management purposes. For instance, LAI maps are used in agro-meteorological models to derive the crop water needs (an example of operative application is given in Irrisat) [20], to monitor the nitrogen status and to apply fertilizer with variable rates (e.g., FarmSat), as input in crop models to derive agronomical variables [21, 22]. On a larger scale, LAI and other biophysical variables are used, amongst others, for yield predictions at administrative level [23, 24, 25]. A general overview of remote sensing contributions to agriculture is given in [26], EO contributions to irrigation practices are listed by Schultz [27].

One application of EO technologies (and the focus of this thesis) is the assessment of water requirement of crops. The water requirement of a plant is predetermined by meteorological conditions and the plant's potential to transpire water. The spatial and temporal knowledge of the crop water requirements can be used for addressing the question of irrigation water require-

ments. The potential of transpiration of crop subtracted by the amount of precipitation results in the amount of water that needs to be artificially supplied by irrigation systems to avoid water stress and achieve optimum yield conditions (for more details see Chapter 2). Estimations of water requirements through ground-based technologies lack the actual real-time measurement of crop development over space. Current estimations of Marchfelds water consumption for agricultural irrigation are based on measurements of the ground water level or post-hoc measurements of applied irrigation and do therefore not measure the real crop water requirement.

To operationally optimize water use and therefore agricultural output, data about vegetation and meteorological conditions have to be obtained contemporary to irrigation practices. This can be achieved by monitoring the spatial distribution of crop parameters over the growing season by time-series of satellite acquisitions.

The aim of this thesis is the calculation and mapping of crop water requirements for the Marchfeld region during the vegetation period of 2010.

As a first step Landsat-5 imagery and agrometeorological data was acquired in the Marchfeld-Region. The satellite-imagery was used to estimate the extent of agricultural surface area. A classification was used to differentiate winter and summer crops. Furthermore multi-temporal VI maps were calculated through satellite imagery. These maps and additionally meteorological data were applied to estimate the potential evapotranspiration (ET_p) for the area. Secondly effective precipitation (P_e) was calculated from records of precipitation using data from local agrometeorological stations. In a last step the information was combined to obtain the seasonal water requirement for cropped surfaces in the Marchfeld-Region.

The methodology offers the possibility to assess the crop water requirement and its spatial and temporal distribution for (agricultural) vegetation. This information can be used to support water management at catchment scale and to cross check the yearly water exploitation plans.

Chapter 2

Materials and Methods

2.1 Overview

The content of this thesis is the calculation of crop water consumption in the Marchfeld-Region during the year 2010. To perform this calculation the potential evapotranspiration, effective precipitation and the area of cropped surfaces needs to be estimated. Evapotranspiration (ET) is a water loss by evaporation from soil and transpiration from plants and depends on type and status of vegetation, land cover and meteorological conditions. Precipitation is the main water input. The cropped surface area is used to calculate the total covered area and volumes for agricultural crops on district scale.

The calculation of potential evapotranspiration in this thesis follows the Food and Agriculture Organization of the United Nations (FAO) guidelines (FAO-56, see Section 2.3.2). This calculation consists of two main components;

1. The **reference evapotranspiration** (ET_0) which indicates the potential amount of water removed from a standard vegetation surface through the process of evapotranspiration. The varying influencing factors are of meteorological nature (solar radiation, wind speed, temperature, air humidity) which are measured by local weather stations. Crop specific factors (LAI=2.88, crop height=0.12, albedo=0.23) are kept constant in relation to the grass reference surface.

2. The potential of the observed crop to transact the reference evapotranspiration. The capacity of transpiration of a plant is influenced by meteorological and crop specific factors like crop type and its development stage and need to be assessed individually to calculate the respective potential evapotranspiration. In the FAO-56 formulation the crop specific factors combined are represented by the **crop coefficient** (K_c).

Reference evapotranspiration was calculated by the Penman-Monteith equation using meteorological data from a local weather station. For further calculation of potential crop evapotranspiration EO data was used in an analytical K_c estimation introduced by D'Urso [28]. Four Landsat-5 TM images were acquired to observe crop development during the growing period. Two different atmospheric correction software applications for satellite imagery were applied (FLAASH - Fast Line-of-sight Atmospheric Analysis of Spectral Hypercubes and ATCOR - Atmospheric Correction). Their performance was evaluated using pseudo-invariant-target comparison. For the estimation of K_c. LAI and Albedo are needed. Crop height was set to a fixed value. LAI values for the Marchfeld area were derived by estimation from spectral reflectance using the CLAIR model [29]. For calibration reference measurements from the 2012 growing season were used. A set of different techniques was applied to calibrate and validate param-

eters needed for the calculation. Albedo values were derived from Landsat-TM data through the "wavelength integrated ground reflectance" by calculating the relative contribution of each band to the total measured energy for each pixel. The influence of albedo, crop height and LAI on the K_c calculation was investigated by a sensitivity analysis.

K_c and ET_0 data was combined to calculate ET_p on a pixel basis. Effective precipitation (P_e) was calculated as a range between minimum and maximum estimations.

The total water requirement of Marchfeld was calculated. The images were first masked to agricultural surfaces only by using the CORINE land-cover map [30]. Then the image time series was used to differentiate winter and summer crop. In a final step the water requirement for summer cropped surfaces of the Marchfeld-Region was determined.

The workflow of the methodologies applied in this thesis is presented in Figure 2.1.

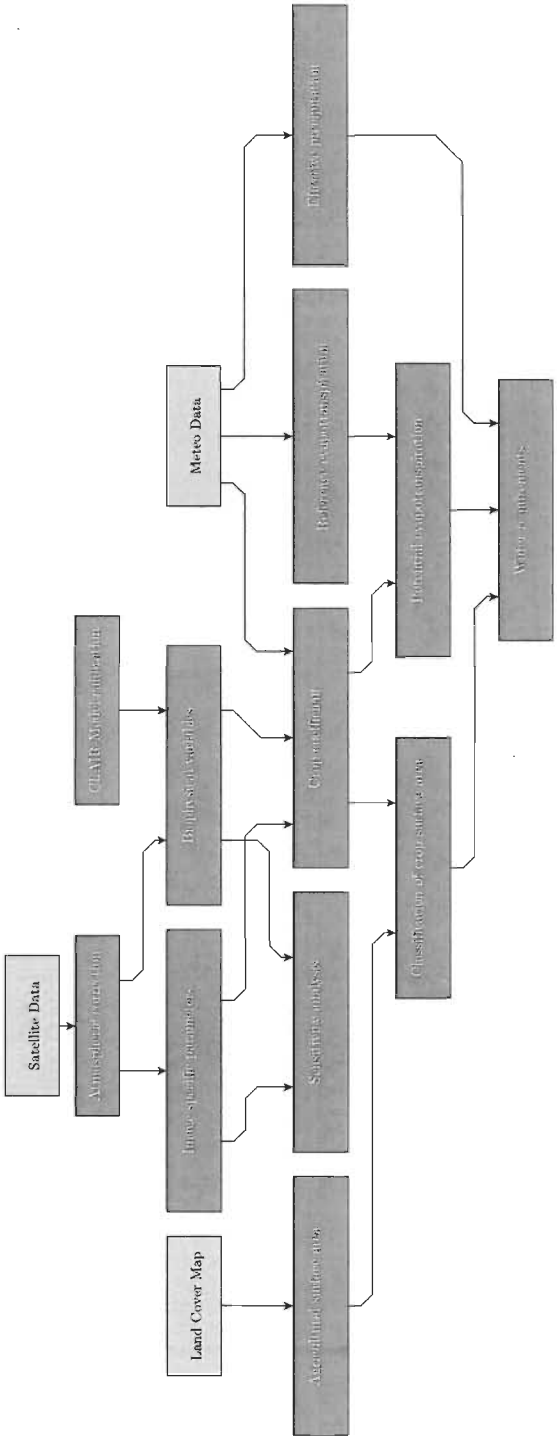

Figure 2.1: Workflow of the methodology

2.2 Test Site Description

Marchfeld is an area in lower Austria. It is part of the "Vienna Basin" and 1000 km^2 in size. The area is depicted in Figure 2.2.

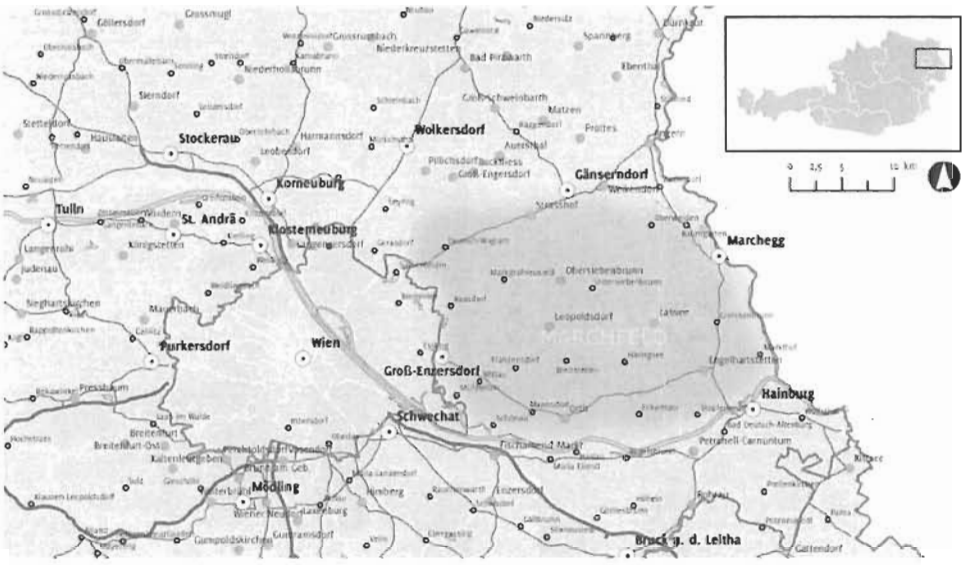

Figure 2.2: Location of the Marchfeld region in Austria.

Climate Marchfeld is located at the western end of the pannonian climate-region. The yearly mean temperature is 10°C and mean duration of sunshine around 1900 hours per year.

The average annual precipitation is 500-550 mm and can drop to 300 mm making it the driest region of Austria. Annual precipitation during the vegetation period (April-September) is 200-440 mm. Dry periods (time with no daily precipitation higher than 5 mm) of three weeks can occur averagely 5 times per year, longer dry periods of 30-34 days are a yearly occurrence [31]. Modelling of future climatic development for Marchfeld and its surrounding regions suggest a decrease of precipitation volumes and an expected increase of likelihood for drought events [10, 11, 12, 13, 14]. High average wind speeds of about 3,5 m/s have an amplifying effect of the dry climate considering plant transpiration. The climate chart of the year discussed in this thesis is presented in Figure 2.3.

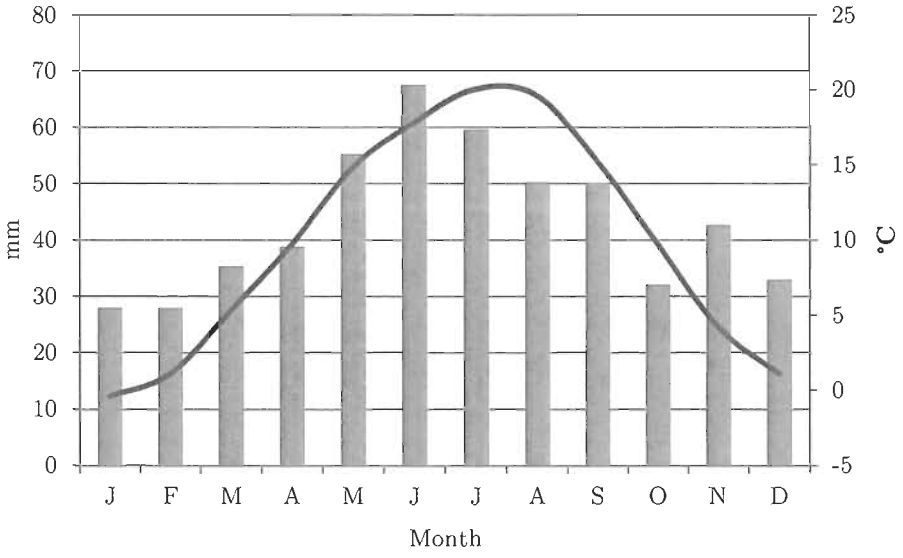

Figure 2.3: Climate chart for the Marchfeld Region for the year 2010. Data from: ZAMG, Weather Station Groß-Enzersdorf

The dominant soil types are Chernozem and Fluvisol, based on the Food and Agriculture Organization (FAO) World Soil Classification. The general soil conditions are characterized by a humus-rich A horizon and a sandy C horizon, followed by fluvial gravel from the former river bed of the Danube [32].

Agriculture The soil consists mainly of fertile aeolian slit deposit which, together with the pannonian climate, high solar radiation and flat terrain forms a well qualified region for agricultural purposes. Limitations to agricultural performance are low precipitation and a predominantly low field capacity of 70 mm and less. This means that the soil can hold only a low amount of precipitation thus limiting water supply to the plants in dry periods. The need for water varies between crops and development stages. Wheat and sugar beet are sensitive to water shortage in the beginning of the vegetation period whereas Maize encounters most limitations during the flowering period. About 65.000 ha of the area in Marchfeld are used for agricultural production. The main crops are vegetables (11%), sugar beet (10%) and potatoes (7%).

Although Marchfeld is the driest regions in the state, it is still one of the primary producers of agricultural goods in Austria. This is possible due to irrigation techniques used by farmers to compensate lacking amounts of precipitation. In Marchfeld most of the water used for irrigation is taken from the ground water. However modernization and intensification of the agricultural sector has resulted in a unbalance of groundwater extraction and replenishment. Thus the groundwater levels in the Marchfeld region have dropped steadily (see Figure 2.4)

The drop of groundwater levels has a profound impact on its surroundings. These impacts range from ecological disturbance over limitations in water use to economical restriction in the agricultural production. To counterbalance the problem of dropping groundwater levels

Figure 2.4: Development of Groundwater levels - Deutsch-Wagram 1940-2001. *Source: Marchfeldkanal*

the Marchfeldkanal-Project was initiated and executed between the years 1986 and 2004. This channel system is used to extract water from the Danube river and transport it to the Marchfeld Region. The main goals of this project were to maintain a secure supply of water to the area, increase water quality, flood control and revitalisation of flowing water bodies.

The construction consist of 100 km of Channels and 8 weirs which control surface water flow and height. To control ground water levels 22 pumping stations and 7 infiltration basins are implemented. In addition the area is equipped with a control system and power supply. An overview of the channel system is given in Figure 2.5. In standard operation the rate of inflow ranges from 0.5 to 7.6 m^3/s. As a result of higher water demand the rate of inflow can rise up to 15.2 m^3/s during the growing season [31]. The cost of construction was 207,8 Million Euro [33].

Irrigation With only 525 mm of precipitation per year additional water supply is needed to sustain stable agricultural production in Marchfeld. Of the 65.000 ha used for agriculture, 30% are irrigated every year. The main water supply for the irrigation system is the groundwater body. The withdrawal from groundwater for agricultural purposes is estimated to be 20-40 Mio. m^3 per year [34].

Irrigation facilities (pumps, infrastructure) are managed on a municipal level. Water is taken either from the channel system or from groundwater. The main mode of irrigation is the "Hose-Reel Irrigator" (Figure 2.6). Sprinkler irrigation systems are also in use, but to a much lesser extent mainly in areas where water pressure of the supply system is not sufficient for hose-reel irrigation.

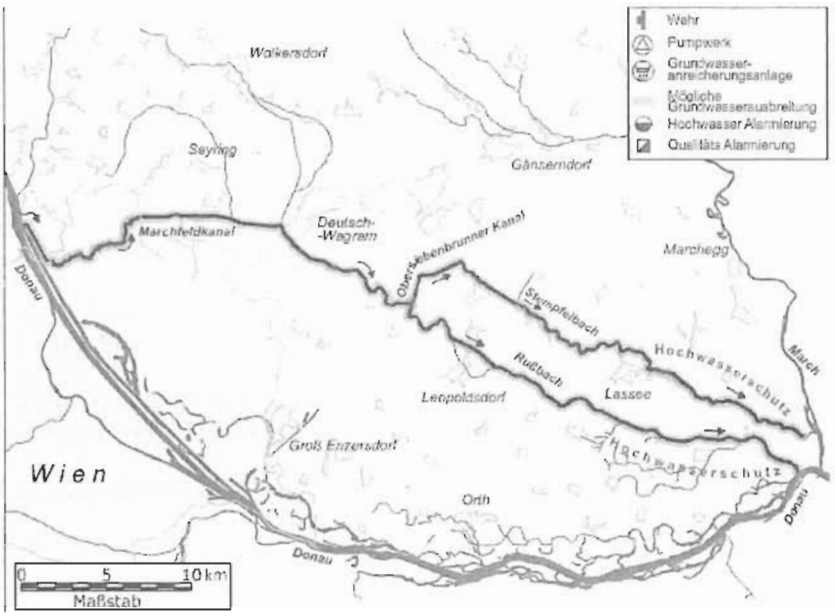

Figure 2.5: Overwiew of the Marchfeld Area including channel system. *Source: Marchfeldkanal*

Figure 2.6: A Hose-Reel irrigation system, which is commonly applied in Marchfeld. Model: Bauer Rainstar

2.3 Calculation of crop evapotranspiration

2.3.1 Introduction to crop evapotranspiration

The calculation of potential evapotranspiration (ET_p) is performed through the crop coefficient approach presented in the FAO-56 paper [35] with the integration of satellite data into the calculation as proposed by D'Urso [28]. The two main components in this concept are the reference evapotranspiration (ET_0) and the crop coefficient (K_c).

The calculation of ET_p is obtained as follows;

$$ET_p = ET_0 \times K_c$$

The methodology assumes *"disease-free, well-fertilized crops, grown in large fields, under optimum soil water conditions, and achieving full production under the given climatic conditions"* [35].

The **reference evapotranspiration** (ET_0) is the evapotranspiration of a standardized vegetated surface area for given climatic conditions within a specified time interval. For details see Section 2.3.2.

The **crop coefficient** (K_c) is a factor indicating the ratio of potential evapotranspiration of crops compared to the reference evapotranspiration. It is defined as

$$K_c = \frac{ET_p}{ET_0}$$

A K_c value of 1 means the evapotranspiration of an observed crop is at the same level as the standard reference surface (grass). A K_c of 1.2 means the evapotranspiration is 20% higher. The primary effects that distinguish crop from the reference surface are

- Crop height
- Albedo
- Canopy resistance
- Evaporation from soil

K_c can be estimated from measurements of actual evapotranspiration and the comparison to the reference evepotranspiration of the standard surface. Using this methodology K_c has been calculated for different conditions and can be provided in tables for several crops. As the K_c changes with crop development it can be displayed as a K_c-curve over time. In the FAO-56 publication these are are provided for each crop development stage as follows: initial stage ((K_{cini}), mid-season stage (K_{cmid}) and end of the late season stage (K_{cend}) (see Figure 2.7).

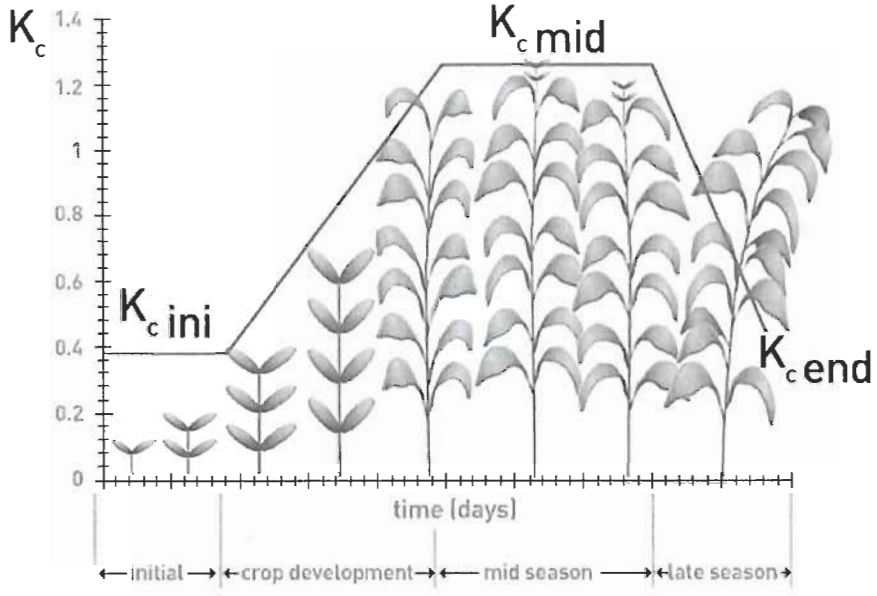

Figure 2.7: Development stages of an exemplary crop and the corresponding developement of K_c over time. *[35]*

Some examples of K_c values within the FAO-56 guideline are given in Table 2.1.

Table 2.1: Reference values of K_c for different crops in three developement stages

Crop	Initial Stage	Mid-season Stage	Late Stage
Sugar Beet	0.35	1.2	0.7
Maize	0.3	1.2	0.5
Winter Wheat	0.6	0.6	0.9
Soy Bean	0.5	1.15	0.5
Potato	0.5	1.15	0.5
Onion	0.7	1.05	0.75

Presented tabulated data represent a fixed value suitable for comparing crop types under general conditions. Crop development is subject to change regarding to local conditions and its climate. An indication of possible variability is given in Figure 2.8. The development of Maize for example can vary between K_c values of 1.1 to 1.4 in full crop development regarding to the climatic conditions it is cultivated in.

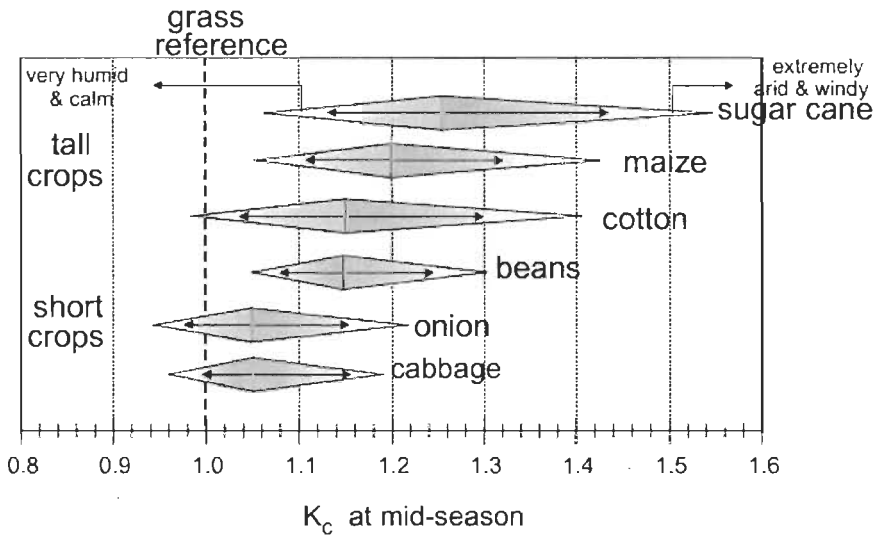

Figure 2.8: Ranges of possible K_c values for full grown crops under variation of climatic conditions *[35]*

The variability of actual K_c to tabulated data further increases when regarding not only climatic differences but also variation in soil type, seeds and management practices.

Figure 2.9 is an illustrated example for the difference from tabulated to actual data. The sample plot of sugar beet in the Marchfeld-Region does not reach the maximum value of K_c=1.2 given by the FAO and is also reaching the senescence stage earlier.

For a precise estimation of water requirement on regional scale the K_c-value must therefore be dynamically adapted to the study area. In this work, the calculation of K_c is achieved by calculation through satellite data.

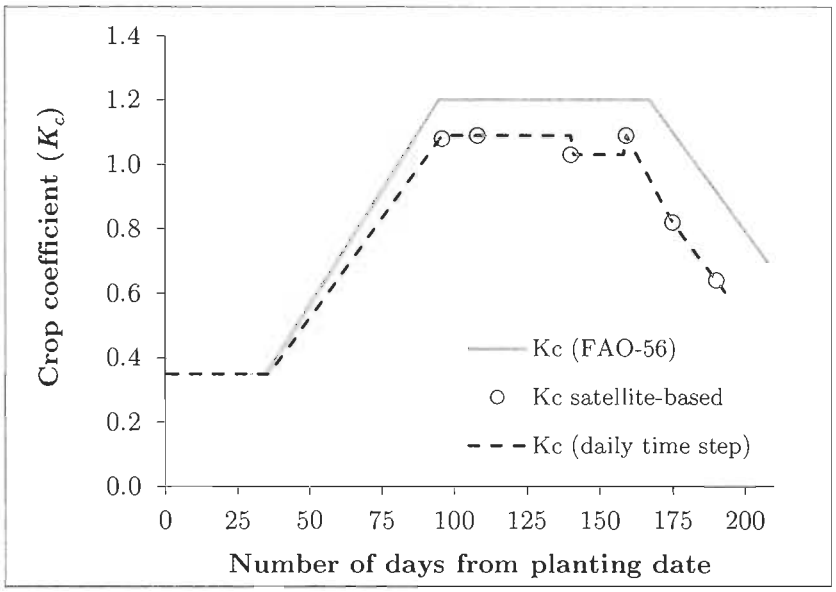

Figure 2.9: Developement of K_c values for a sample plot of sugar beet in the Marchfeld-Region and the FAO-reference of K_c developement for the same crop

2.3.2 Reference Evapotranspiration

The reference evapotranspiration was derived from meteorological data with the use of the Penman-Monteith equation. It is physically based and incorporates physiological and aerdoynamic parameters [35].

Penman-Monteith equation

$$ET_0 = \frac{0.408\Delta(R_n - G) + \gamma \frac{900}{T+273} u_2 (e_s - e_a)}{\Delta + \gamma(1 + 0.34 u_2)}$$

where
ET_0=reference evapotranspiration [mm day^{-1}],
R_n=net radiation at the crop surface [MJ m^{-2} day^{-1}],
G=soil heat flux density [MJ m^{-2} day^{-1}],
T=mean daily air temperature at 2m height [C],
u_2=wind speed at 2m height [m s^{-1}],
e_s=saturation vapour pressure [kPa],
e_a=actual vapour pressure [kPa],
e_s-e_a=vapour pressure deficit [kPa],
Δ=slope vapour pressure curve [kPa C^{-1}],
γ=psychrometric constant [kPa °C^{-1}].

In summary ET_o is a function of: **Meteorological Data**

- Radiation
- Temperature
- Relative Humidity
- Windspeed
- Evaporation from Soil

Crop specific data

- Leaf Area Index
- Albedo
- Crop Height

The meteorological data is measured in-situ with weather stations. For the reference evapotranspiration (ET_0) the crop specific factors are set to LAI=2.88, Albedo=0.23, h_c=0.12.

Source for meteorological data was the Zwerndorf weather station operated by the "Zentralanstalt für Meteorologie und Geodynamik". ET_0 estimations for this weather station have been cross-checked with another nearby weather station.

2.4 Satellite Data

2.4.1 Earth Observation-Data Description

EO datasets were acquired by two satellites; Landsat-5 TM data was used for the calculation of the water consumption. For this calculation a calibrated model is needed to obtain LAI maps. For this purpose, a calibration campaign was conducted in 2012 where ground reference LAI-measurements were taken in correspondence to DEIMOS-1 image acquisition. Both datasets were geometrically corrected by the data supplier. Landsat-5 TM records data with the Landsat Thermatic Mapper (TM)-Sensor in 7 bands with a spatial resolution of 30 m (in the visible, near- and shortwave infrared bands) and 120 m (thermal). DEIMOS records data in 3 spectral bands with a spatial resolution of 22 m. Table 2.2 shows the dates of the image acquisitions for the two campaigns

Table 2.2: Dates of image acquisition used for the estimation of crop developement (Landsat-5) and calibration of model parameters (DEIMOS-1)

Landsat-5	DEIMOS-1
10.06.2010	17.06.2012
12.07.2010	30.06.2012
22.08.2010	01.08.2012
23.09.2010	20.08.2012
	05.09.2012
	18.09.2012

2.4.2 Data preparation

Due to the fact that the atmospheric conditions have a varying influence over time and space a correction to account for these effects has to be applied. Two different software tools for atmospheric correction (FLAASH and ATCOR) were considered and their performance tested. FLAASH and ATCOR are two different software-modules. The aim of these modules is to correct recorded at-sensor signal for atmospheric effects through modelling atmospheric parameters.

Atmospheric Correction

The radiance is recorded as a signal at sensor level. The signal is affected by properties of the atmosphere that lie between the sensor and its observed target. Since atmospheric properties are dynamic, the recorded at-sensor reflectance of a surface will be subject to variation. The variations are of temporal (variation from one image acquisition to another) and spatial (variation within a single image) nature. Furthermore a part of the radiation recorded at the sensor is reflected by the atmosphere directly with no interaction of the observed surface (backscattering). The backscattered signal carries no information about the surface area and should be eliminated for further processing.

There are different ways to perform atmospheric correction. The influence of the atmosphere can be determined with in situ measurements of the surfaces' reflective properties. Another method is to estimate the atmospheric effect on image acquisitions through a model atmosphere. The latter approach was used in this thesis. For the atmospheric modelling a set of model parameters are needed. These parameters are:

- Latitude/Longitude
- Sensor Altitude
- Acquisition Date/Time
- Ground Elevation
- Visibility
- Sensor Calibration

FLAASH is a tool included in the ENVI Image processing software. It is based of MODTRAN4 radiative transfer model. The user interface of the software is presented in Figure 2.10. To apply this correction method imagery data values were converted from digital number to radiance and corrected with current radiometric calibration coefficients (bias and gain) using the formula:

$$L_\lambda = G_{rescale} x Q_{cal} + B_{recale}$$

where
L_λ=Spectral radiance at sensor $[W/m^2 sr\mu m]$
$G_{rescale}$=Band-specific gain factor $[W/m^2 sr\mu m/DN]$
Q_{cal}—Band-specific rescaling bias factor $[W/m^2 sr\mu m]$

Bias and Gain factors are contained in the imagery metadata.

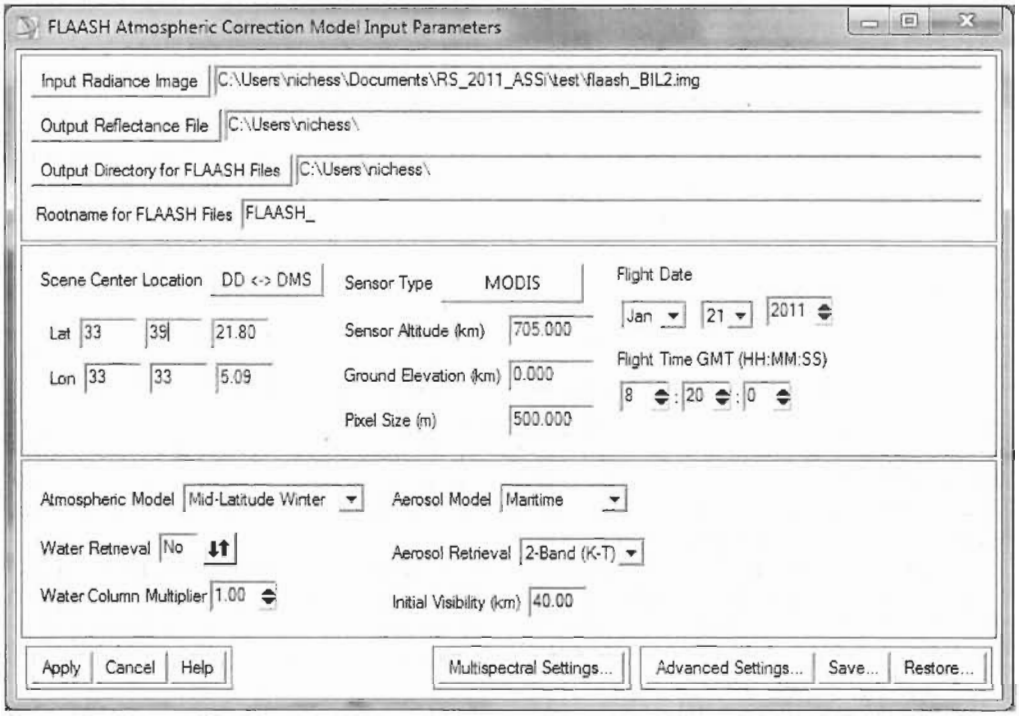

Figure 2.10: The user interface for the model input parameter within the FLAASH atmospheric correction tool

Resulting top of the atmosphere (TOA) radiance values were then used as input to FLAASH. The result was an estimation of top of the canopy (TOC) reflectance values.

ATCOR is also based on MODTRAN4 and is a module in the ERDAS Imagine software. Additionally to an application of model atmosphere and its parameters, ATCOR allows the iterative choice of the model parameters to match the corrected pixel reflectance with the observed reflectance from a spectral library or from user measurements. The user interface for comparison of reflectance is presented in Figure 2.11.

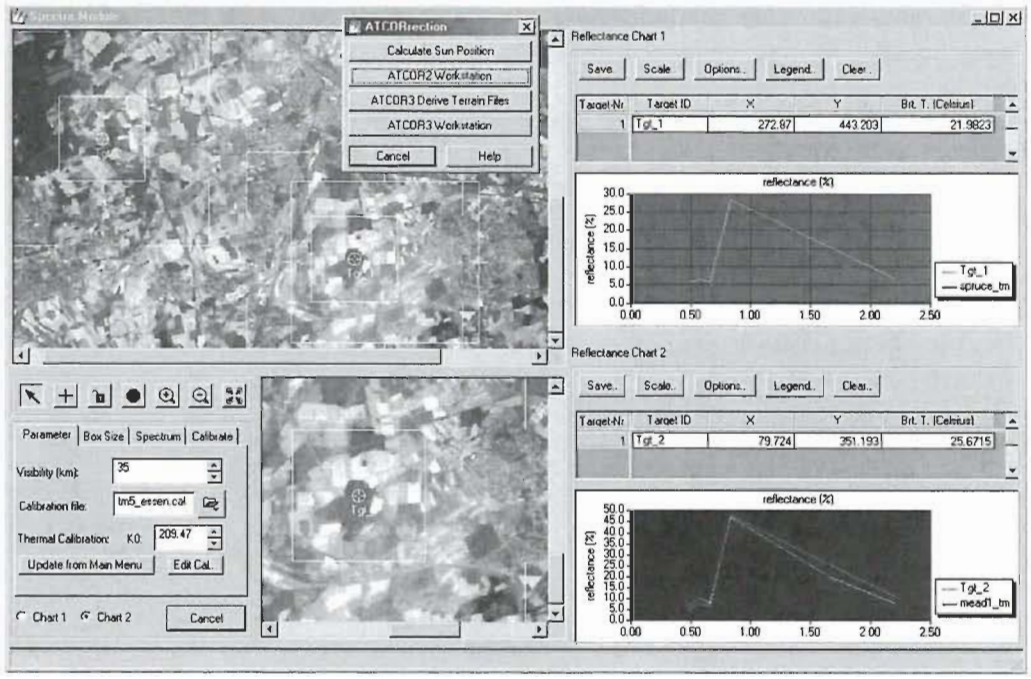

Figure 2.11: The user interface for check and adjustment of model input and performance within the ATCOR atmospheric correction tool

Comparison of Atmospheric Correction Methods

To compare the two correction approaches a set of pseudo invariant targets (PITs) was selected. The assumption is that spectral response from invariant targets stay the same over time thus making it possible to compare the performance of atmospheric correction methods. The necessary characteristics of pseudo-invariant targets are [36], [37]:

- Targets should be available with both high and low radiance
- Targets should be as homogeneous as possible
- They should be smooth and horizontal to minimize shadow and directional effects.
- They should be of large size, to minimise adjacency effects and make them easy to identify on different images, and on the ground.

To compare the correction methods the standard deviation of spectral response of a single target over time was measured.

2.4.3 Data Processing

The aim of EO data processing is to derive K_c maps for the observed area which are further used for the estimation of potential evapotranspiration. EO based K_c values were calculated using the approach described by D'Urso [28] . For the estimation of K_c, LAI, albedo and crop height are needed.

Calculation of the leaf area index LAI

LAI was derived through the Weighted Difference Vegetation Index (WDVI) as follows [29]:

$$LAI = \frac{1}{LAI_\alpha} ln(1 - \frac{WDVI}{WDVI_\infty})$$

In this equation two coefficients (LAI_α, $WDVI_\infty$) need to be calibrated. The calibration of LAI_α was done using ground reference measurements and contemporaneous image datasets from the year 2012. The full process is described in Appendix A.

Calculation of weighted differential vegetation index WDVI

WDVI can be calculated from EO data as presented by Clevers [29]:

$$WDVI = \rho NIR - C \times \rho R$$

The soil line slope (C) represents the slope of the linear relationship between bare soil reflectance observed in two different wavebands [38]. It was calibrated by a number of samples (60 in this study) of bare soil per image. From the respective reflective values in the red and near-infrared bands of each sample the soil line slope was derived according to the following equation.

$$C = \frac{\rho NIR}{\rho R}$$

The intercept was set to 0.

Calculation of albedo

Albedo is defined as the ratio of the reflected radiation of a surface to the incoming radiation. Albedo depends on the type of surface and angle of incidence of solar radiation. A high reflective surface like fresh snow may reach an albedo of 0.95. Low values of 0.05 are common for wet bare soils. Vegetation has an albedo of 0.20-0.25 [35].

Albedo is used in the calculation of the fraction of solar radiation (R_s) that is not reflected from the surface (net solar radiation - R_{ns}) with $R_{ns} = (1 - \alpha)R_s$.

The calculation for the albedo is done by deriving the relative contribution of each band to the total measured energy for each pixel. In this operation the surface albedo is substituted by the "wavelength-integrated ground reflectance" since the recorded spectral data only covers part of the full spectral region. This operation was performed within the ATCOR module of ERDAS Imagine. The formula applied to derive the wavelength-integrated ground reflectance is:

$$a = \frac{\int_{0.3\mu m}^{2.5\mu m} \rho(\lambda) d\lambda}{\int_{0.3\mu m}^{2.5\mu m} d\lambda}$$

Estimation of the crop coefficient (K_c)

For the estimation of potential evapotranspiration the EO estimated canopy parameters (albedo, LAI, h_c) can be directly introduced to the FAO Penman-Monteith equation replacing the standard values of the grass reference surface (see Section 2.3.2). This directly estimates the potential ET. Because of its wide use in irrigation practice, it is useful to derive a physically-based basal

crop coefficient K_c expressed as an explicit function of crop parameters and of meteorological data. Assuming a constant crop height the (polynomial) function relating K_c to albedo and LAI is:

$$K_c = (a_4 + b_4 \times r)LAI^4 + (a_3 + b_3 \times r)LAI^3 + (a_2 + b_2 \times r)LAI^2 + (a_1 + b_1 \times r)LAI + (a_0 + b_0 \times r)$$

where
r=Albedo[%]

The coefficients a and b are derived by calculating ET_p with meteorological data at the time of the satellite image acquisition and averaging out the resulting K_c for a period of 5-6 days around the date of the image acquisition [39].
Crop height (h_c) controls the resistance in canopy aerodynamic properties. Measurements of exact crop heights for large areas and over a time period of several months are not feasible due to considerable work load. Therefore the crop height was set to a fixed value, which is considered to be a satisfactory compromise in estimation of ET_p [39]. In this methodology the crop height was set to a value of 0.3 m. Since in reality crop height is variable over time its influence was investigated by performing a sensitivity analysis of K_c to h_c. The variation of K_c with six different h_c-values over a range of LAI was calculated. This was done by deriving a and b coefficients for crop heights of 0.1 m, 0.2 m, 0.25 m, 0.35 m, 0.5 m, 0.75 m and 1 m. Their corresponding K_c values were calculated and its variation plotted. A similar sensitivity analysis was performed on variations of albedo. An estimation of K_c with a constant h_c of 0.5 and increasing LAI was done with variation of albedo ranging from 0.1 to 0.4.

Finally, we estimated the crop water requirement. This was achieved by subtracting effective precipitation (P_n) from the potential evapotranspiration. If ET_p surpasses P_n vegetation enters a stage of water deficit. To achieve optimal crop development and yield conditions this deficit that has to be balanced out by applying irrigation.

The crop water requirement (CWR) can be expressed as

$$CWR = ET_p - P_n$$

Effectiveness of precipitation relies on a number of factors such as: crop type, crop condition, soil conditions, irrigation scheduling, characteristics of the precipitation events (duration, intensity, frequency) etc. Since a number of these factors are inaccessible for a regional estimation of water deficit the effective precipitation is estimated as a range. The lower end of effective precipitation (less water is assimilated by the plant) is given above (P_nmin). The upper end (P_nmax) was set to:

$$P_nmax = P * 0.75$$

The lower end of effective precipitation was calculated by applying following formula:

$$P_nmin = (P - 5) * 0.75$$

where
P=Precipitation [mm]

Estimation of agricultural surface area

Image classification was used to estimate the cropped area for summer crops in the Marchfeld region. As a first step all non-agricultural (urban & natural surfaces, forest, water bodies) surfaces were masked. This was done by using the "Corine Land Cover Map" (CLC-Map) which holds information of EO based estimation of landcover and usage. A subset of the CLC-map for Marchfeld is presented in Figure 2.12. The CLC-Map was reprojected to UTM WGS '84 with overlapping pixel features to imagery data of Landsat (pixel size of 30m). The next step was to perform an unsupervised classification. The image acquired on August 22nd was selected. The choice for this data was driven by the circumstance that agricultural summer crop are expected to be well developed at this time and therefore easily distinguishable from surrounding land cover types. Seven clusters were initially selected. The classification was followed by a visual interpretation of the different clusters using a false-color composite image of the region. During this analysis the clusters were separated into vegetation or soil. One cluster resulted in uncertain classification and was further analysed visually based on the crop coefficient. The visual interpretation of K_c was done in regard of value, location and extent.

For further processing two types of area estimations were defined: **(1) "General Agricultural Area"** incorporates all agricultural surfaces, sparse and dense vegetation as well as soil into the calculation.

(2) "Cropped Surfaces" incorporates all pixels clearly classified as "vegetation" , border-effects (mixed-pixels) were excluded. This procedure represents an estimation of irrigation crop water requirements of the region.

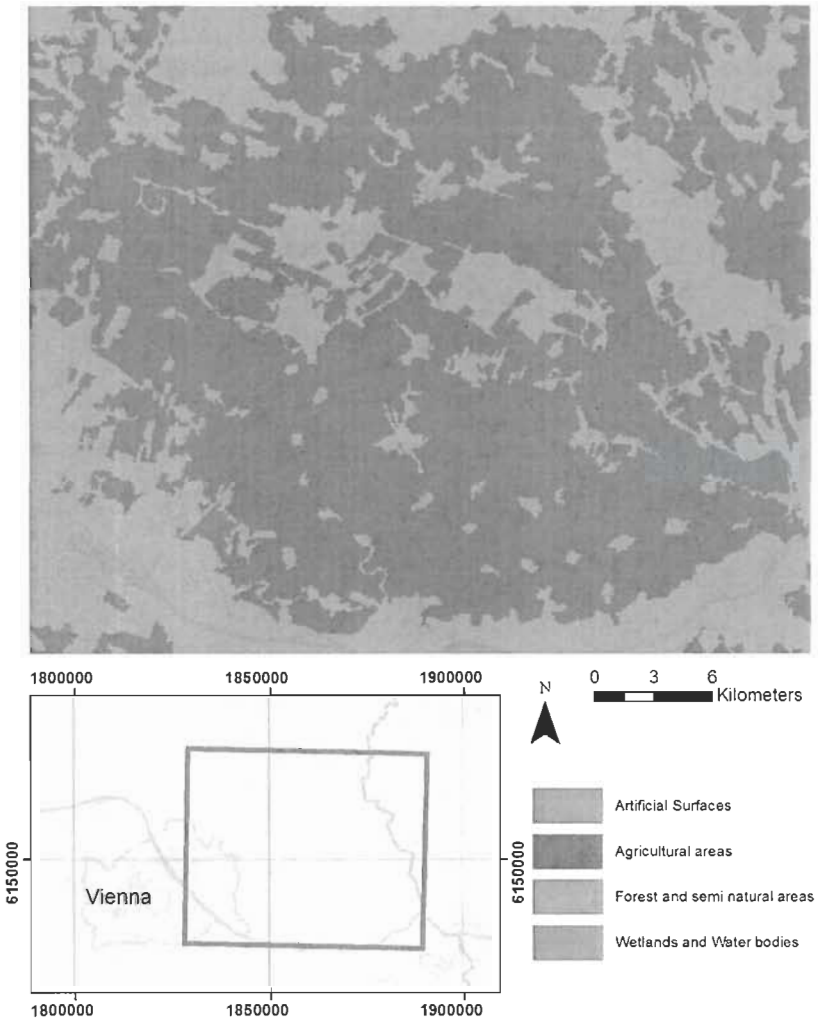

Figure 2.12: A subset of the Corine Land Cover map for the Marchfeld Region. Classes were aggregated to 4 categories.

2.5 Calculation of potential evapotranspiration and water requirement

For the calculation of crop water requirement the raster based K_c value was interpolated to obtain daily K_c values. This resulted in 106 (daily) K_c values from 10th of July to 23rd of September. A daily estimation of ET_p was calculated by multiplying interpolated K_c values with ET_0 of the respective day. The result is a raster file with pixel based estimation of ET_p with 106 layers corresponding to each day from the first image acquisition to the last. A total sum of ET_p for each pixel was calculated. 10-day time-step ET_p aggregations were used to calculate the water requirement for the areas. Effective precipitation values were aggregated in the same 10 days time-steps and subtracted from the ET_p estimations. The result is the magnitude and temporal development of crop water requirement for the observed area

Chapter 3

Results and Discussion

In the following chapter the results of the methodology are presented and discussed. All tables and figures are located adjacent to the discussion.

3.1 Reference Evapotranspiration

The reference evapotranspiration (ET_0) for the Marchfeld Region in 2010 ranges from 0.07 mm/day (27. Dec. 2010) to 6.64 mm/day (13. July 2010) with an average of 2.13 mm/day over the whole year (see Figure 3.1). The highest reference evapotranpspiration was taking place in July with an ET_0 of 148.5 mm/month. January exhibits the lowest value with 12.8 mm/month. Summarized monthly values of ET_0 are presented in Figure 3.2. The highest values of ET_0 are located in the mid-summer months. Low values of ET_0 during this period are due to cloud-coverage, low temperatures and other unfavourable condition. Notable is the high variability of ET_0 during the summer months. Unfavourable meteorological conditions in June can result in the same ET_0 as days in March or October. The estimation of ET_0 was within the expected range of observed climatic conditions.

The results of ET_0 calculation from weather data recorded at Zwerndorf were compared to the calculation for data recorded at Groß-Enzersdorf. The two weather stations are approximately 26 km apart. For the observed time period the differences in the estimations reaches a maximum of 122.5% on the 25th. of July where Zwerndorf recorded ET_p=1.18 and calculation from Groß-Enzersdorf weather data resulted in ET_p=2.63. Analysis of the weather data for Groß-Enzersdorf showed higher temperature (+0.6 °C), a higher wind-speed (+1.4 m/s) and lower air humidity (-10 %) during that day. Similar variations can be observed for other high divergences. On average the calculation of ET_p from Groß-Enzersdorf during the image acquisition campaign was 2.16 % higher, with a standard deviation of 20.42 %.

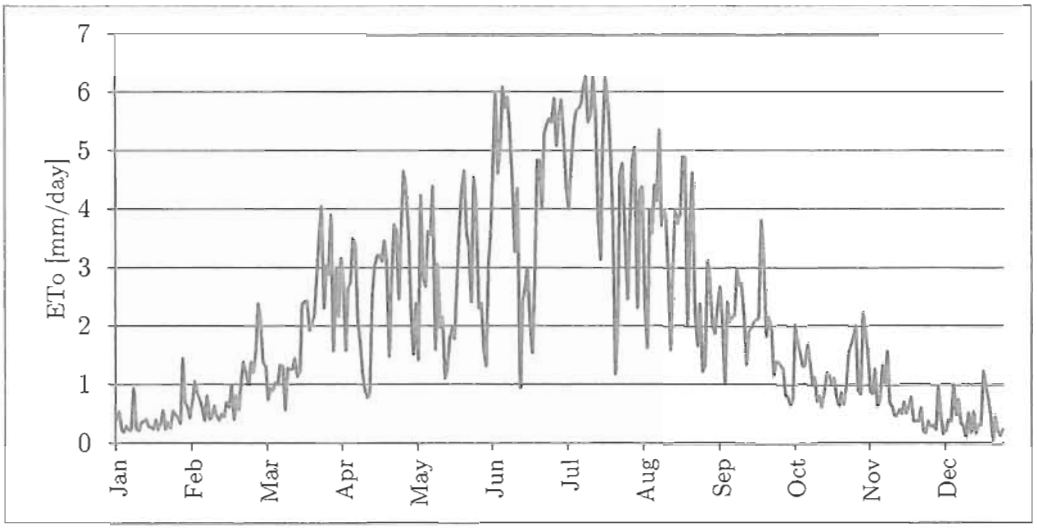

Figure 3.1: Daily reference evapotranspiration (ET_0) for the year 2010 calculated from meteorological data collected at Zwerndorf

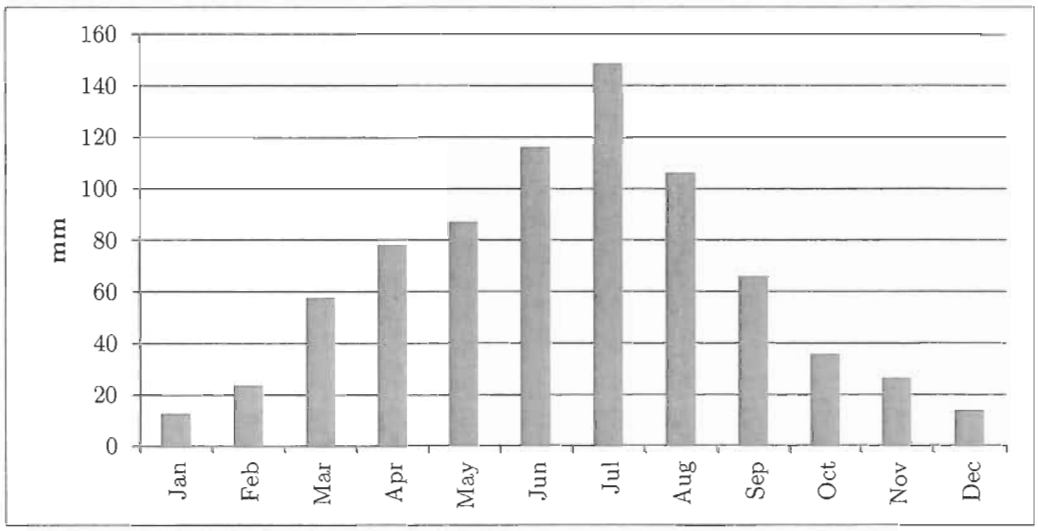

Figure 3.2: Summarized monthly evapotranspiration (ET_0) for the year 2010 calculated from meteorological data collected at Zwerndorf

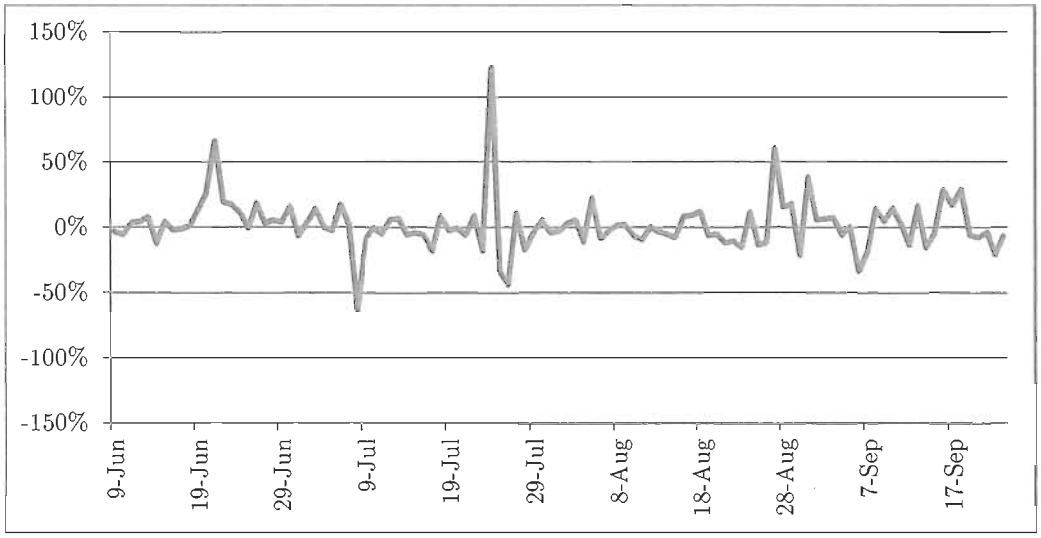

Figure 3.3: The percentage difference of calculated reference evapotranspiration (ET_p) when comparing meteo data recorded at Zwerndorf to ET_p-calculation from Groß-Enzersdorf data. The timeframe is 10. of June to 23. of September

3.2 Satellite Data

3.2.1 Pre-Processing - Atmospheric Correction

Band specific spectral reflectance

When analysing the reflection of a vegetated surface, atmospheric correction changes the recorded reflectance the most in the 0.45-052 μm region (Band 1 - blue). In this band a decrease can be observed after applying atmospheric correction. A similar, but smaller effect takes place in band 2 (green) and 3 (red). With Band 4 (NIR) the effect is reversed and the recorded reflectance percentage after correction is higher than TOA recorded values (see Figure 3.4). For analysis of a non-vegetated surface the spectral refletance profile of a stone quarry was used (see Figure 3.5). Except for band 1 (blue) reflectance responds with an increase of values after performing atmospheric correction on TOA data.

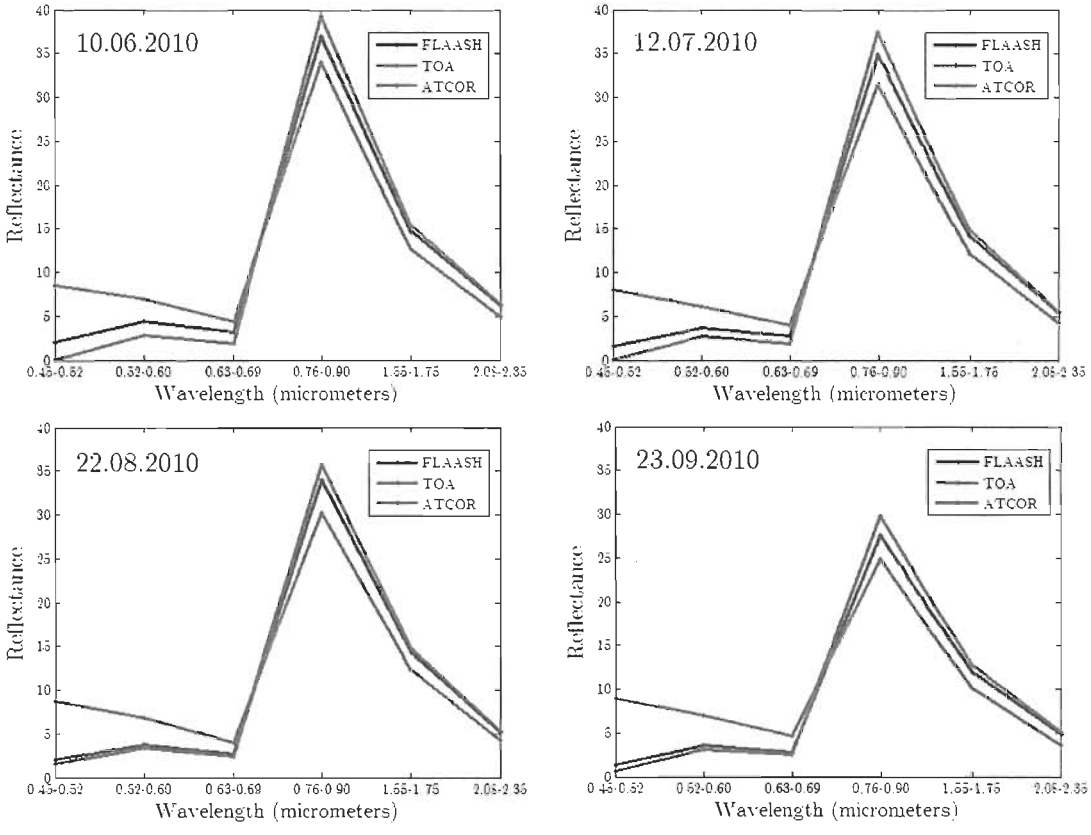

Figure 3.4: Spectral profiles for reflectance [%] with and without atmospheric correction for PIT # 5 (Forest canopy) taken from four different image acquisitions

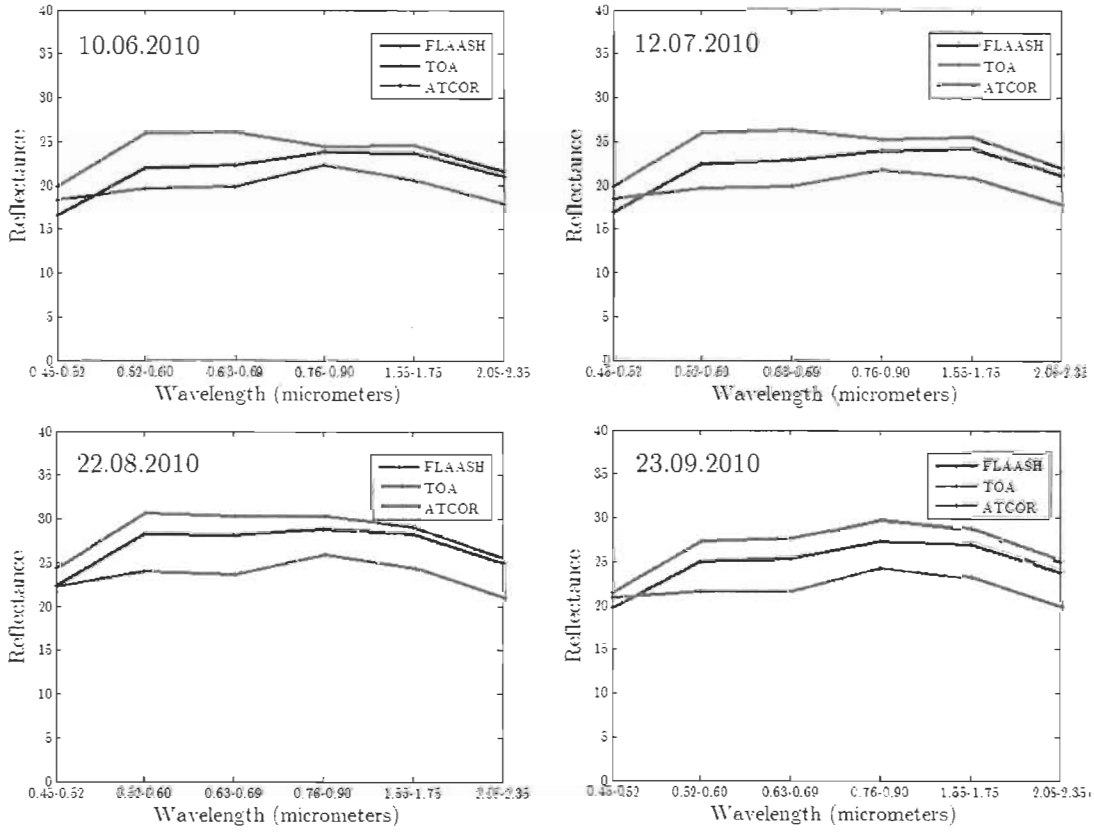

Figure 3.5: Spectral profiles for radiance [%] with and without atmospheric correction for PIT # 9 (Stone quarry) taken from four different image acquisitions

Stability of atmospheric correction using pseudo-invariant targets

The standard deviation of PITs over time was used to estimate the performance of atmospheric correction methods.

The Tables from 3.1 to 3.3 shows the Standard Deviation of PITs over time for 3 different scenarios; Table 3.1 shows top of the atmosphere data, Table 3.2 reports data atmospherically corrected with ATCOR and Table 3.3 reports data atmospherically corrected with FLAASH. Table 3.4 indicates the normalized difference of variability of all targets over the six spectral bands when comparing an atmospheric correction method to top of the atmosphere.

The results showed an increase of variation after the application of both correction procedures. This can be a result of the method used for the analysis and/or an actual limitation of software performance. Regarding the former (method used): some of the variation can be related to actual change of the pseudo-invariant targets that were set on vegetation canopy. This can be observed in Table 3.2 and Table 3.3 where higher percentages of the variation with both models applied are coming from Band 4 of the sensor used when comparing to other bands. Observed variation in the near-infra-red band is most likely due to actual changes in the plant canopy during the observed time period.

The other reason for an increase in variation might be the selected calibration of model parameters and the performance of the correction method. To achieve better performance of correction methods it is suggested to obtain in-situ measurements during the image acquisition campaign and tune the model parameters in regard of these measurements. Further processing was done with the FLAASH-corrected datasets where the analysis of pseudo-invariant targets showed a lower variation.

Table 3.1: Standard deviations of PIT reflectance over time for top of the atmosphere (uncorrected) imagery

PIT #	Band 1	Band 2	Band 3	Band 4	Band 5	Band 6	average
1	1.29	1.82	2.02	3.38	2.55	1.90	2.16
2	0.82	0.82	0.86	4.53	0.66	1.03	1.45
3	0.47	0.48	0.50	3.88	0.21	0.44	1.00
4	0.74	0.30	0.48	2.29	0.46	0.14	0.73
5	0.43	0.41	0.29	3.87	1.15	0.58	1.12
6	0.41	0.56	1.06	0.88	1.35	1.88	1.02
7	0.27	1.08	1.76	2.71	2.60	2.84	1.88
8	0.41	1.19	1.40	1.75	1.18	1.78	1.29
9	1.95	2.10	1.83	1.90	1.89	1.58	1.87
10	0.47	0.00	0.20	0.55	0.29	0.49	0.33
average	0.73	0.88	1.04	2.57	1.23	1.27	

Table 3.2: Standard deviations of PIT reflectance over time for data corrected with ATCOR

PIT #	Band 1	Band 2	Band 3	Band 4	Band 5	Band 6	average
1	1.87	2.75	2.67	3.99	2.83	2.33	2.74
2	0.38	0.76	0.74	5.54	0.82	1.15	1.57
3	0.30	0.65	0.84	4.49	0.08	0.47	1.14
4	0.71	0.73	0.75	2.37	0.44	0.20	0.87
5	0.70	0.34	0.32	4.12	1.12	0.59	1.20
6	1.24	1.86	2.31	1.61	2.15	2.73	1.98
7	1.89	3.18	3.75	3.40	2.91	2.92	3.01
8	1.64	2.74	2.96	2.02	1.24	1.73	2.05
9	2.14	2.24	1.95	2.97	2.28	2.06	2.27
10	0.54	0.45	0.57	1.53	0.43	0.61	0.69
average	1.14	1.57	1.69	3.20	1.43	1.48	

Table 3.3: Standard deviations of PIT reflectance over time for data corrected with FLAASH

PIT #	Band 1	Band 2	Band 3	Band 4	Band 5	Band 6	average
1	1.93	2.56	2.54	3.92	2.79	2.33	2.68
2	1.24	1.29	1.18	5.09	0.84	1.16	1.80
3	0.11	0.13	0.41	4.21	0.09	0.38	0.89
4	0.34	0.25	0.31	2.23	0.34	0.18	0.61
5	0.36	0.32	0.21	4.04	1.21	0.61	1.12
6	0.64	0.98	1.30	0.90	1.79	2.42	1.34
7	0.88	1.67	2.16	3.05	2.96	3.05	2.29
8	0.88	1.48	1.56	1.70	1.05	1.77	1.41
9	2.72	2.95	2.66	2.53	2.18	1.97	2.50
10	0.11	0.29	0.15	0.87	0.46	0.60	0.42
average	0.92	1.19	1.25	2.85	1.37	1.45	

Table 3.4: Normalized difference of variability of PIT reflectance when comparing TOA reflectance to atmopsherically corrected data (ATCOR and FLAASH correction)

	Band 1	Band 2	Band 3	Band 4	Band 5	Band 6	average
ATCOR	0.57	0.79	0.62	0.24	0.16	0.17	0.43
FLAASH	0.27	0.36	0.20	0.11	0.11	0.14	0.20

3.2.2 Data Processing

Calculation of albedo

Albedo values within the processed imagery are varying within 2% in the case of water pixels and 80% in the case of clouds. The histogram shows a peak around an albedo value of 10% which corresponds with soils and urban structures. Mean values and standard deviations are reported in Table 3.5.

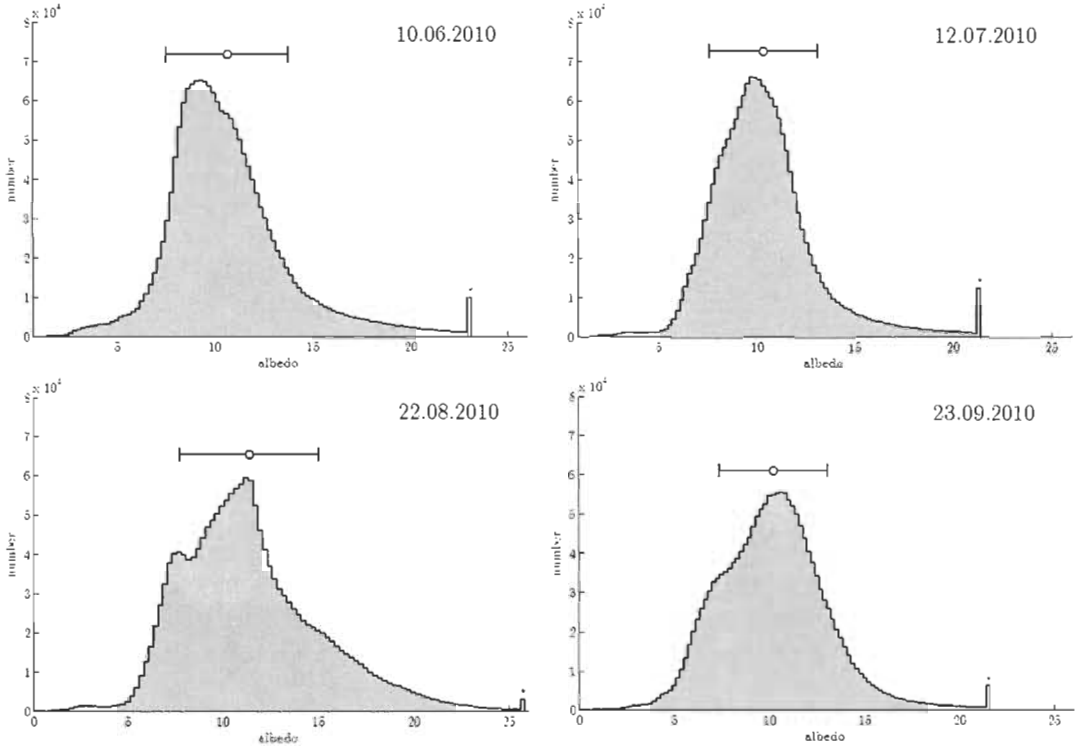

Figure 3.6: Histograms for the raster based albedo calculation for four image acquisitions

Calculation of the leaf area index (LAI)

The performance of different calibration techniques was validated with LAI ground reference measurements. A detailed description of the approach used was published by Vuolo et al. [40] and can be found in the appendix to this thesis.

Using the CLAIR model with an image-specific tuning of the soil line slope and $WDVI_{\infty}$ and a constant LAI_{α} coefficient value provided the most accurate and consistent results for WDVI based LAI estimation (R^2=0.64, RMSE = 0.86). The other validated calibration techniques included seasonal average (constant) values for the soil line slope, $WDVI_{\infty}$ and LAI_{α} (R^2=0.58, RMSE = 1.04) and image-specific model parameters for each image acquisition (R^2=0.54 to 0.78, RMSE = 0.97 to 0.53 depending on the individual imagery datasets).

Calculated LAI values range from 0 to 6. A visualisation of pixel based LAI calculations for July 12th is given in Figure 3.8. The mean value of LAI over the region of interest varied with the season due to vegetation development, land cover dynamics and cultivation practices from LAI_{mean}=1 (23.09.2010) to LAI_{mean}=1.9 (10.06.2010). Modulation of model parameters and results of the LAI calculation are presented in Table 3.5. The distribution of LAI values in the region of interest are presented in Figure 3.7. One can observe a considerable shift to low LAI values in the histogram when comparing the first to the second image acquisition. The observed variation is due to senescence and harvest of winter wheat, a primary agricultural product of the region. A second peak around an LAI of 1.5 and 3 appear in the third and forth image. This is due to subsequent greening up of summer crops and secondary crops following on plots antecedently used for winter crop cultivation.

Table 3.5: Calibrated parameters for the calculation of WDVI and LAI and resulting mean values and standard deviations of resulting LAI calculation for each image acquisition respectively

	Model parameters			Albedo		LAI	
Date	**Soil Line Slope**	**LAI_{α}**	**$WDVI_{\infty}$**	**mean**	**σ**	**mean**	**σ**
6/10	1.38	0.34	52	10.63	3.13	1.94	1.04
7/12	1.34	0.34	56	10.34	2.75	1.30	1.06
8/22	1.32	0.34	56	11.38	3.62	1.33	1.10
9/23	1.46	0.34	57	10.20	2.85	1.06	0.87

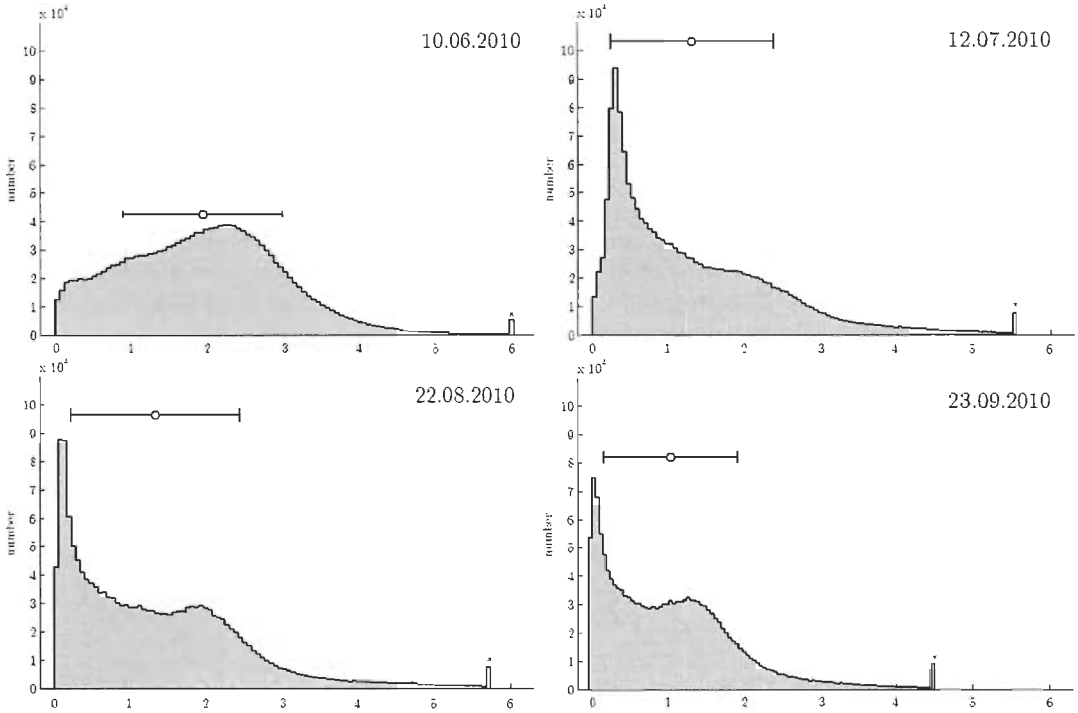

Figure 3.7: Histograms for the raster based LAI calculation for four image acquisitions

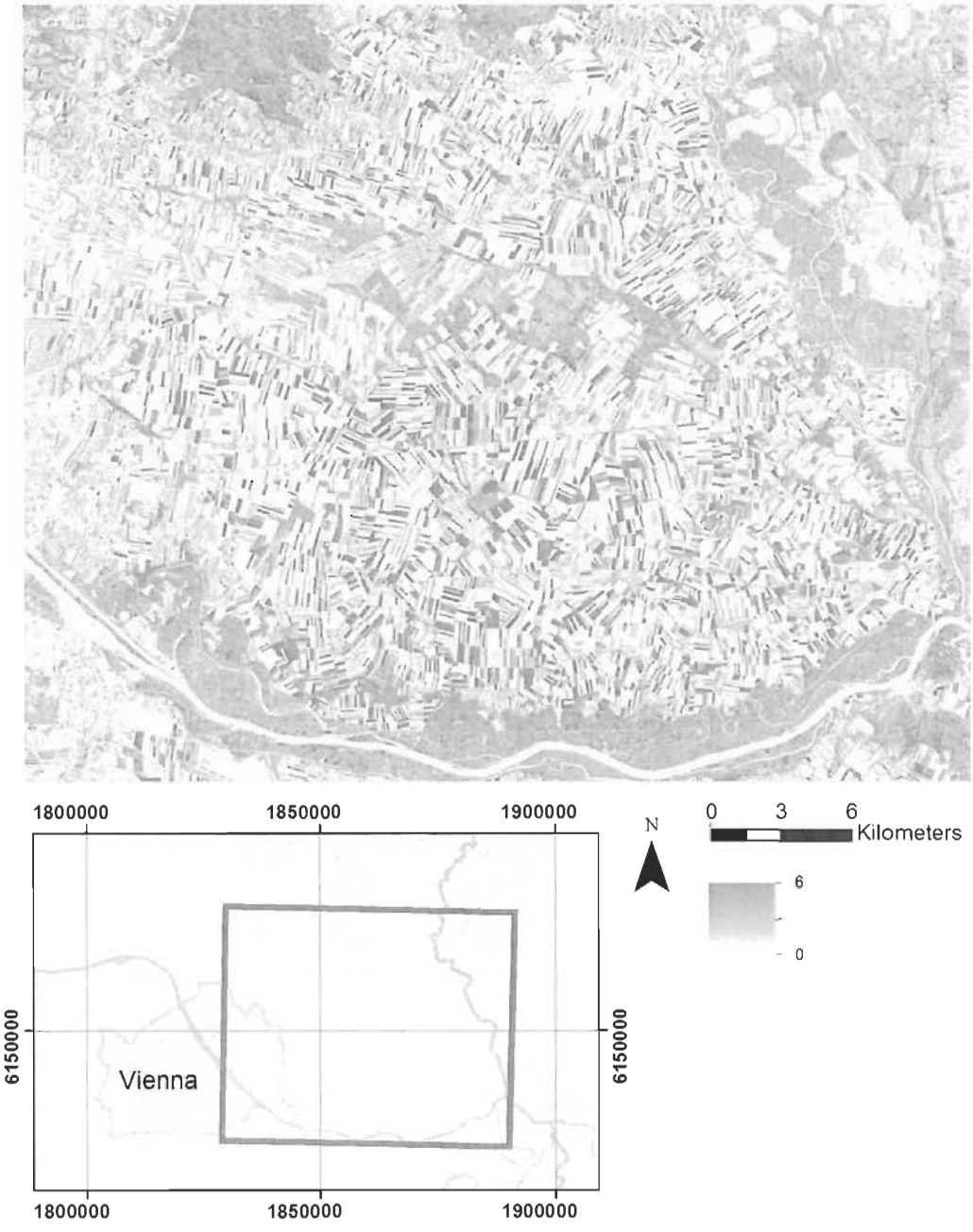

Figure 3.8: Visualization of EO estimated LAI-values for the acquisition on 12.07.2010

Estimation of the crop coefficient (K_c)

Results of the a and b coefficient calibration along with mean K_c values and their standard deviation for the raster image datasets are given in Table 3.6. Histograms of the K_c raster dataset are plotted in Figure 3.9. The calculation of mean values and histograms was done using only the **"agricultural surface area"**. Estimated K_c values range from 0.05 to 1.5. The EO data from June, 6th shows the highest image-wide mean value of K_c=0.97. Mean values of K_c are decreasing over time with the lowest value (K_c=0.53) at the end of the image acquisition campaign. The steady decrease of K_c is a result of crop development and agricultural management. The first acquisition captured winter wheat cultivation during the end stage which responded correctly with high K_c values at the time. Another reason for decreasing K_c is the vegetation cycle with declining vitality of vegetation in September.

Table 3.6: Coefficients for the calculation of K_c and mean values and standard deviation of resulting raster based K_c dataset for each image acquisition respectively

	Calibration coefficients			K_c	
Date	**coefficient #**	**a**	**b**	**mean**	**std**
6/10	**0**	0.0595	-0.0298	0.97	0.33
	1	0.7939	-0.4982		
	2	-0.1855	0.0996		
	3	0.0229	-0.0103		
	4	-0.0013	0.0005		
7/12	**0**	0.1224	-0.0546	0.73	0.38
	1	0.9535	-0.5304		
	2	-0.2946	0.1431		
	3	0.0456	-0.0202		
	4	-0.0028	0.0012		
8/22	**0**	0.0635	-0.0312	0.59	0.43
	1	0.816	-0.4899		
	2	-0.1953	0.0978		
	3	0.0246	-0.0101		
	4	0.0014	0.0005		
9/23	**0**	0.0712	-0.0439	0.53	0.39
	1	0.743	-0.4778		
	2	-0.1534	0.1061		
	3	0.0171	-0.0129		
	4	-0.0009	0.0007		

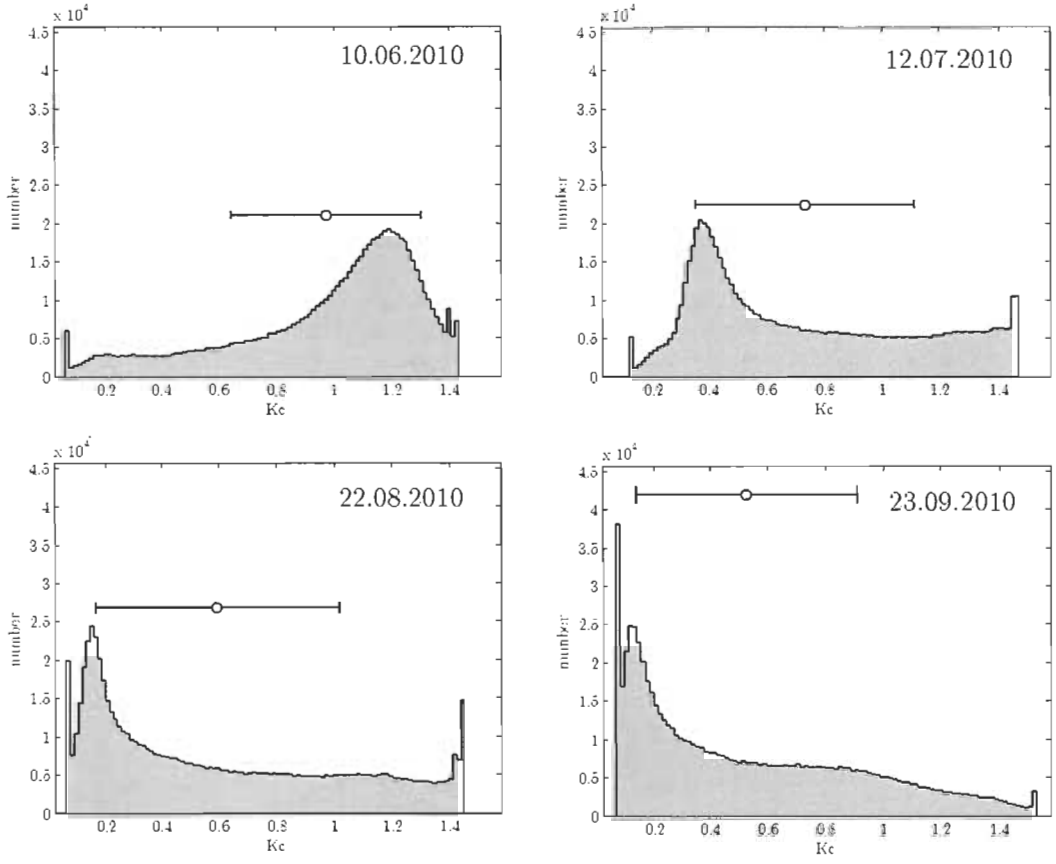

Figure 3.9: Histograms for the raster based K_c calculation for four image acquisitions.

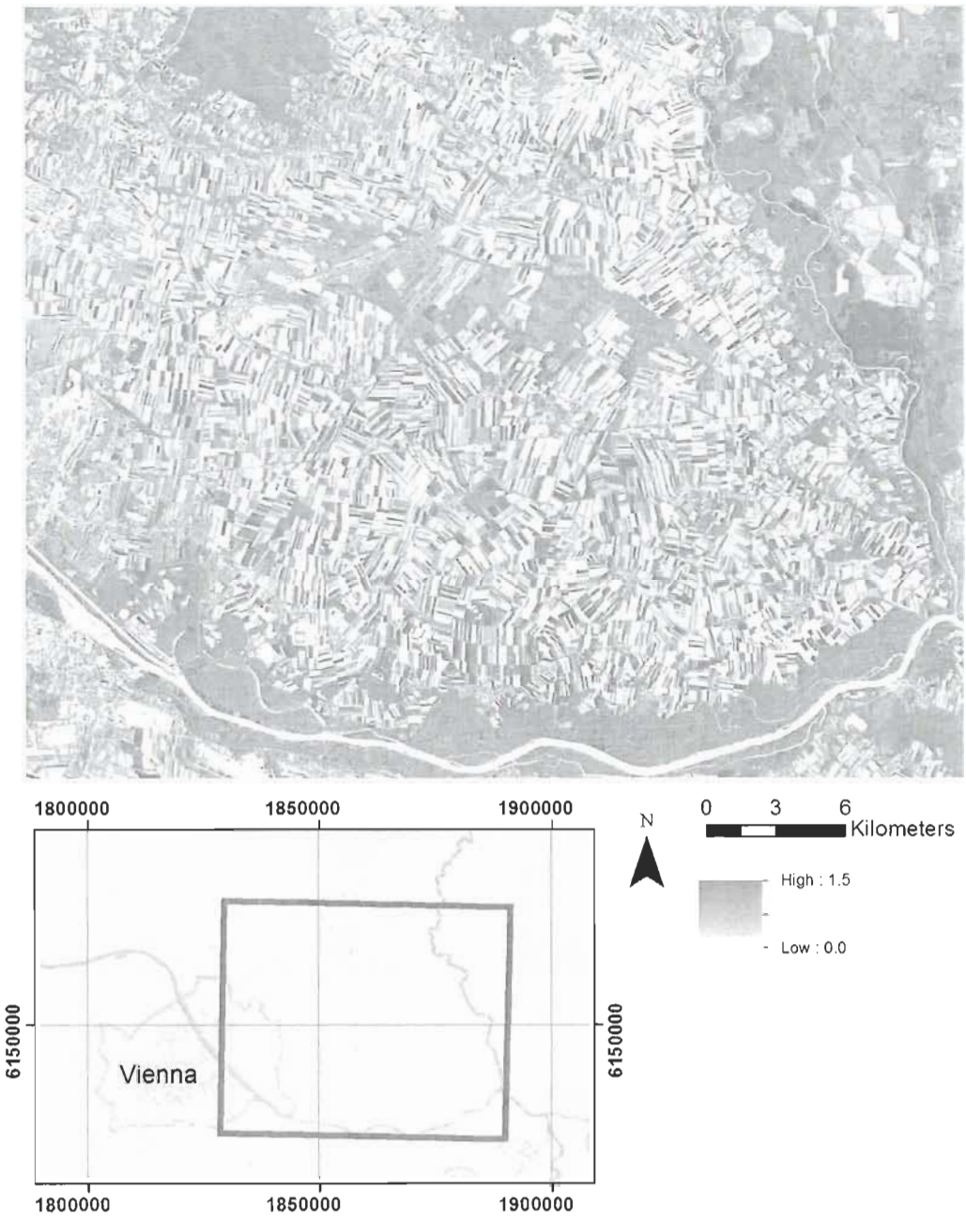

Figure 3.10: Visualisation of K_c-Values for 22.08.2010

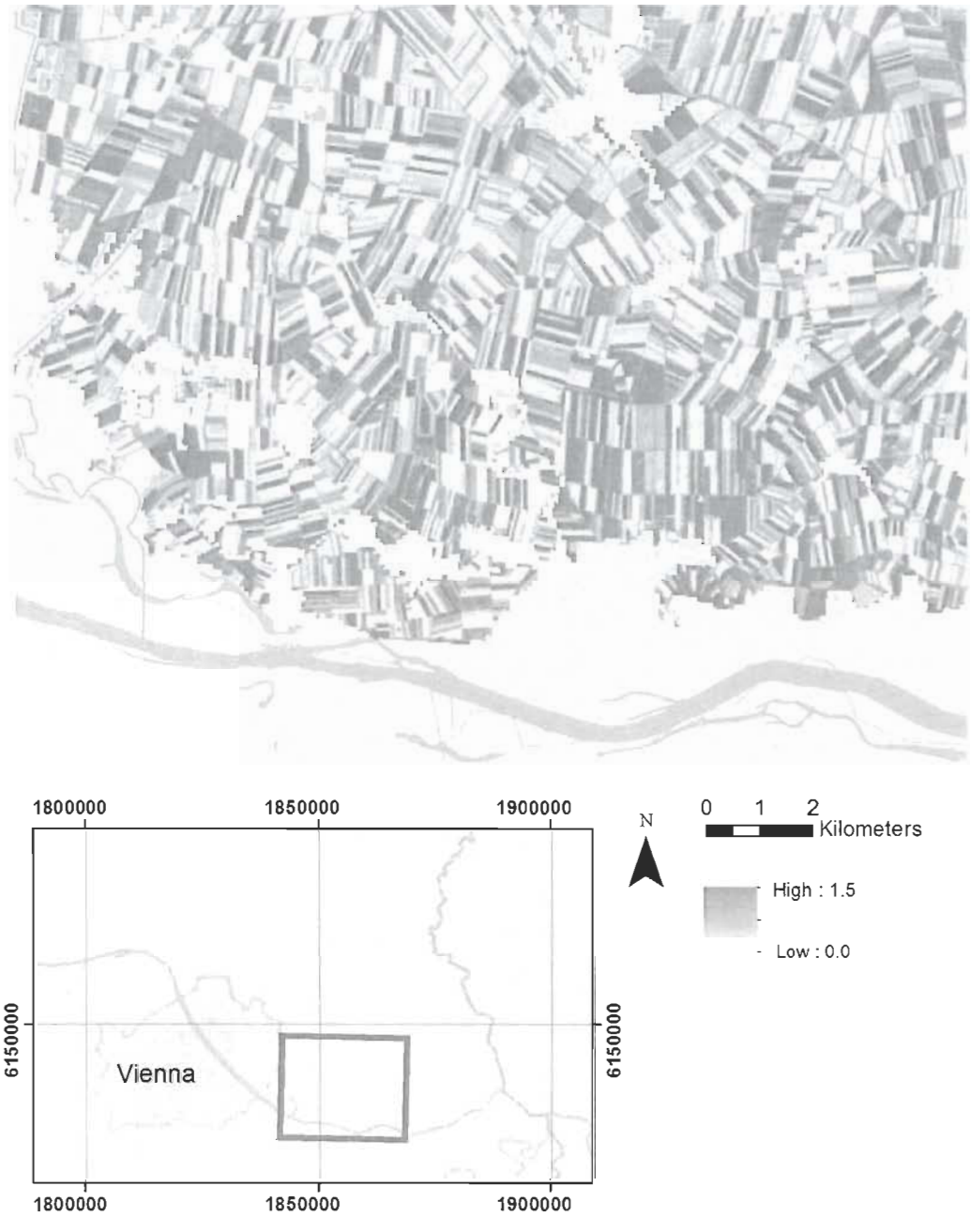

Figure 3.11: Subset of raster-K_c-Values on 22.08.2013 limited to agricultural areas of the Marchfeld-Region

Sensitivity Analysis

Figure 3.12 displays the variation of K_c values when calculated with different input parameters (h_c, LAI). Starting off at the same point the curve is increasing in a slope that has a steeper inclination with higher h_c values. All curves saturate around the LAI value of 5. After this peak a slight decrease is taking place.

The percentage difference of K_c presented in Figure 3.13 is a measure of the influence of variation over LAI. Differences in K_c estimation increase with LAI values and saturate at around LAI=4.5. The results show possible variation of K_c of up to $\pm 0.15\%$ for high LAI values.

A similar, but more regular change can be observed for the variation of albedo values in the estimation of K_c. The variation of albedo for high values of LAI results in a difference of $\pm$ 15% is close to that value ($\pm$ 13%) for low values.

The sensitivity analysis showed that the crop height can influence the estimation of K_c within a maximum range of $\pm$ 15% for high values. Low values of LAI show a much lower variation when applying different h_c-values (for LAI=1; -0.005% to +0.002%). A possible solution to minimize the error is to estimate the h_c over time. To do so additional information about the observed crop (type, sewing date etc.) has to be obtained.

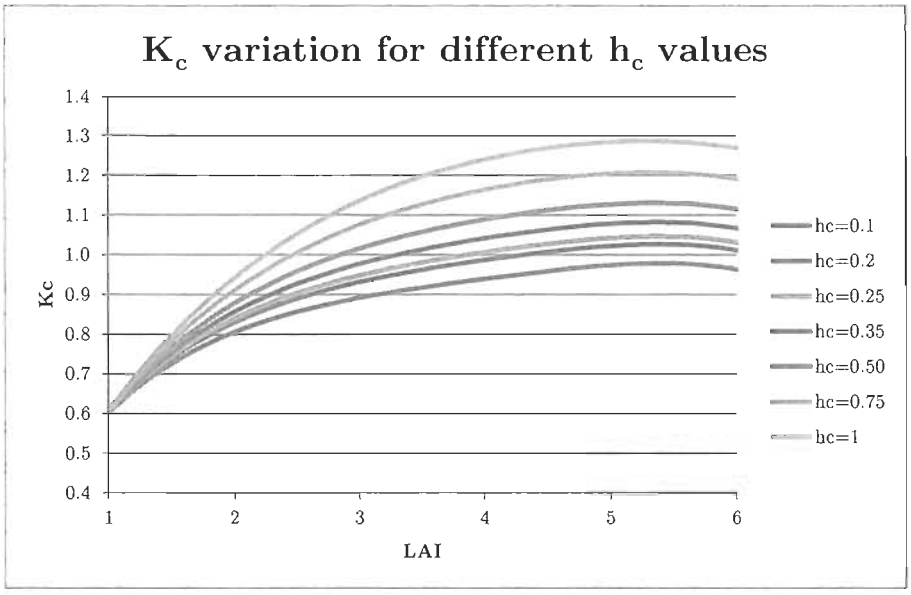

Figure 3.12: The variation of estimated K_c values when calculating with different h_c as input values

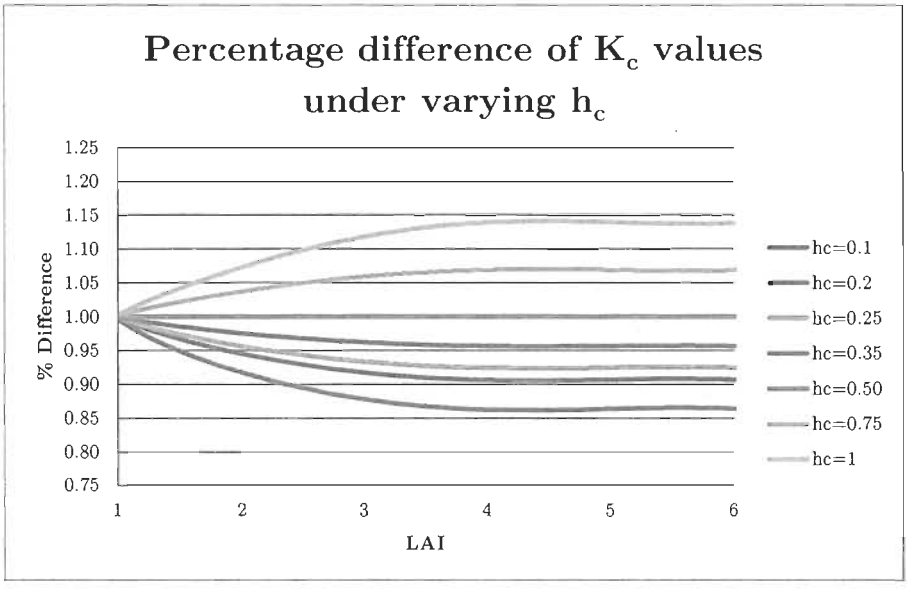

Figure 3.13: Percentage difference of K_c estimations under varying h_c conditions in relation to h_c=0.5

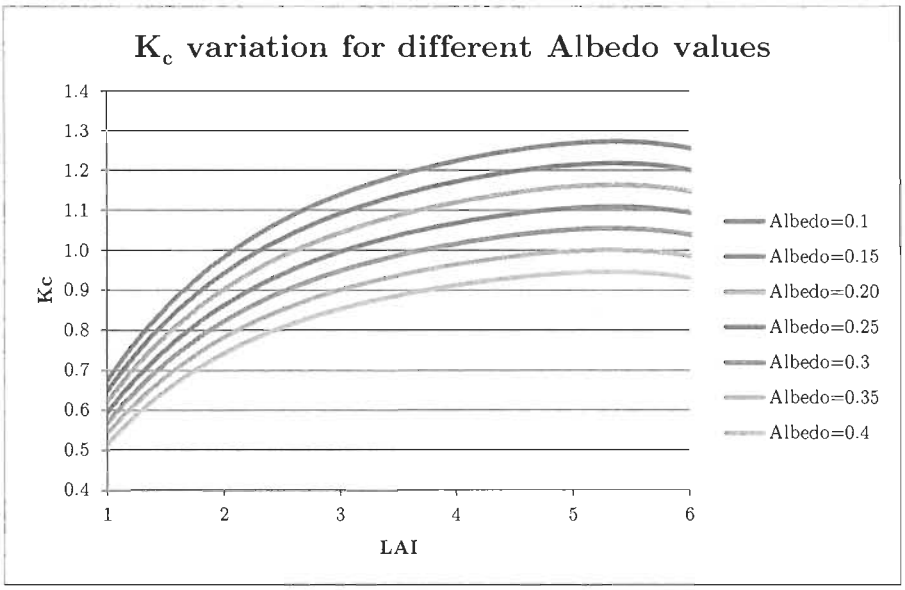

Figure 3.14: The variation of estimated K_c values when calculating with different albedo as input values

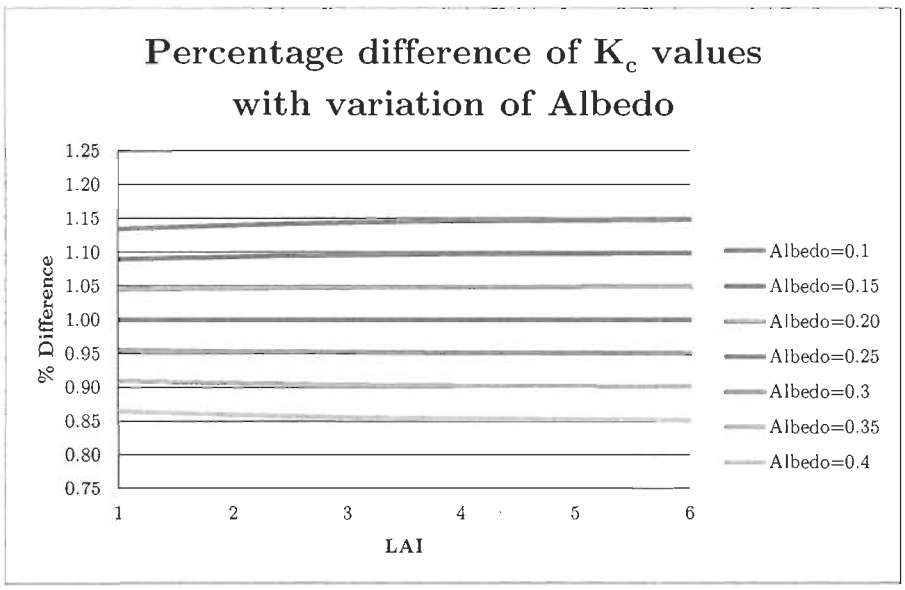

Figure 3.15: Percentage difference of K_c estimations under varying Albedo conditions in relation to Albedo=0.25

Estimation of agricultural surface area

The 7 data clusters obtained from the image unsupervised classification could be identified and grouped in soil and vegetation classes accordingly One cluster remained uncertain and was further investigated. Analysis of K_c values for these areas showed a K_c-variation of 0.01 to 1.1 with a maximum amount of pixels at K_c=0.63. The spatial distribution of pixels in this class showed that it identifies "border-effects" around agricultural fields. (see Figure 3.17) For the estimation of the "cropped surface area" estimation all classes clearly identifiable as vegetation were combined. Mixed-pixels were excluded. "Cropped surface area" incorporated all pixels which are assumed to be dense vegetation on agricultural soil. This dense vegetation is assumed to be a result of irrigation practice (since dense vegetation would not develop with low precipitation).

A subset of the image classification is shown in Figure 3.16. The total surface area is given in Table 3.7. The estimated surface area for general agricultural areas and summer cropped surface are within the expected range when being compared to other reference values which estimate the area extent of summer crops to be around 20 000 ha [41]. 34% of the general agricultural area was used for summer crop ("cropped surface") production in the year 2010.

Table 3.7: Extent of the two types of surface areas classified from satellite data

Surface Type	Area
General Agricultural Area	62933 ha
Cropped Surface	21780 ha

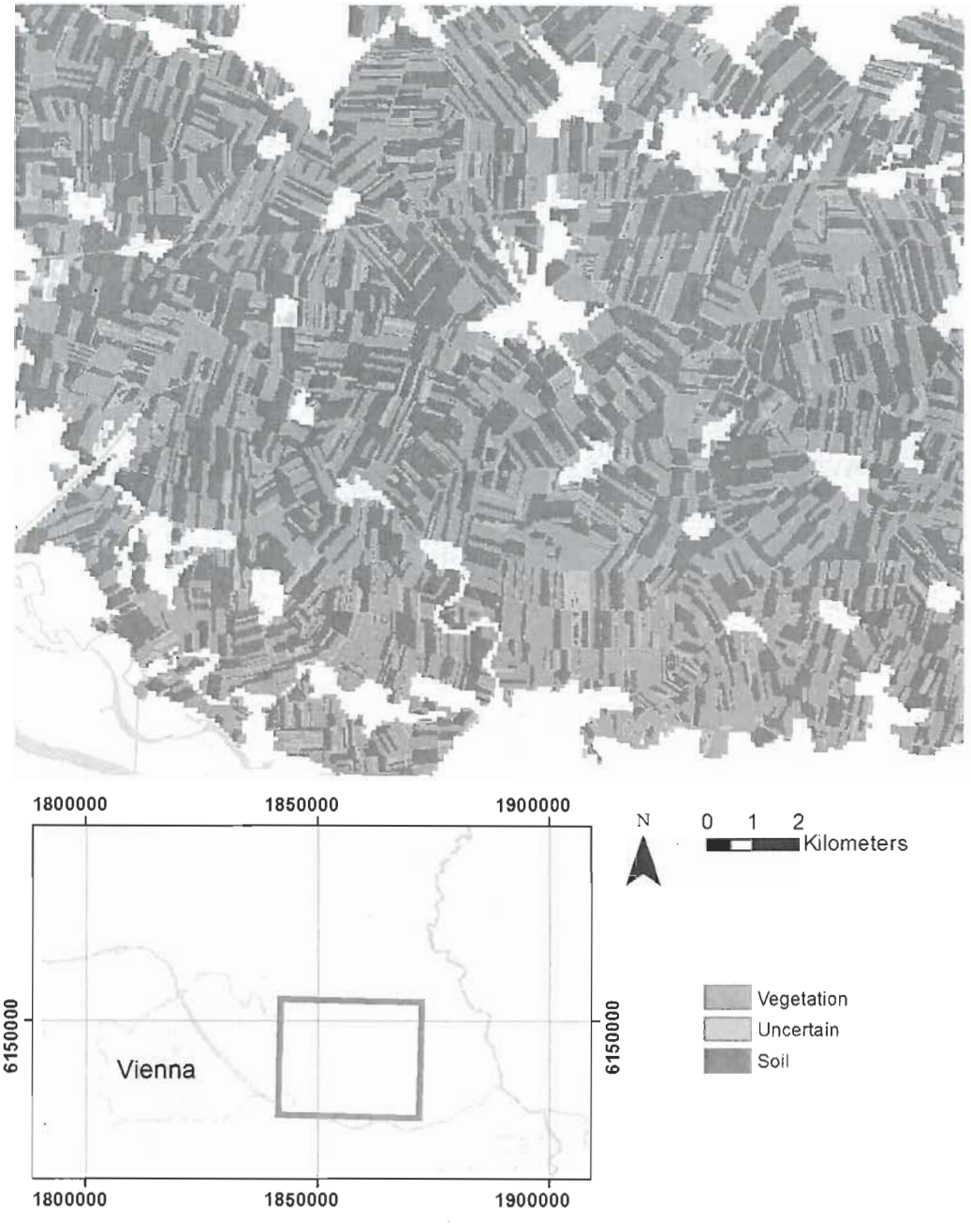

Figure 3.16: Land cover map derived from Landsat-TM Imagery of August 22.

Figure 3.17: A visualization of "Class 4" showing the border effects around fields

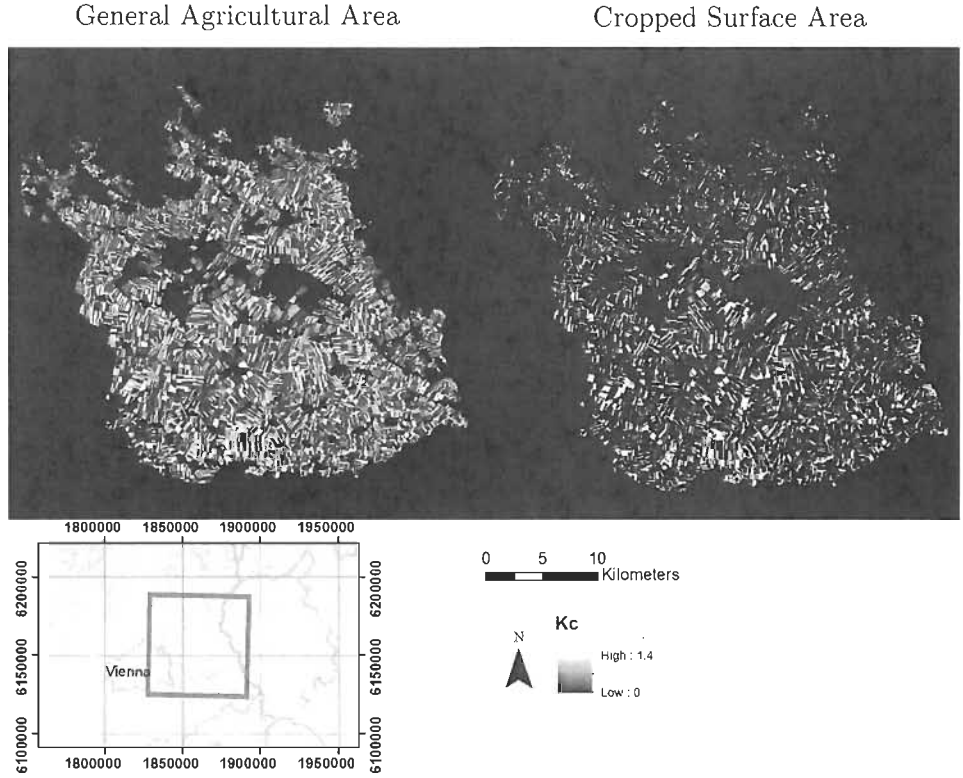

Figure 3.18: Results of 2 the different area estimations displayed as K_c-values on 22.08.2013

3.3 Calculation of potential evapotranspiration

The seasonal evapotranspiration is presented in Figure 3.19. The distribution of values within the region of interest is presented in Figure 3.20. The "General Agricultural Area" responds with a larger amount of pixels for low ET_p values than the "Cropped Surface Area" and vice versa because regions with low potential for evapotranspiration (uncropped surfaces) were masked in the classification process. Fields with high potential evapotranspiration are located throughout the Marchfeld-Area. These fields correspond with overall high K_c values over time as depicted in Figure 3.21 and Figure 3.22. This indicates high plant vigour during the time of the image acquisition campaign, which coincides with the development of summer crops. Winter crops, like winter wheat are covered only in their end- and senescence stage and do thus not contribute decisively to high seasonal ET_p rates. On average, ET_p is 272 mm from June 10th to September September 23rd for the the General Agricultural Area. When analysing the Cropped Surface Area only the mean value is expectedly higher with 398.44 mm (see Figure 3.20). The maximum value is 560mm. This amount of total potential evapotranspiration for 4 months represents closely total precipitation of a full year in this region evidently illustrating the need for irrigation.

For further analysis the daily potential evapotranspiration was aggregated to 10 days time-steps for the "General Agricultural Area" and for the "Cropped Surface Area". The results are given in Table 3.8 and plotted in Figure 3.23. The "Cropped Surface" area shows a potential

evapotranspiration ranging from 58.6 mm/10 days at the end of July to 19.6 mm at the end of the observed time period. The "General Agricultural Area" has an overall lower potential for the evapotranspiration. The maximum is 40.6 mm and the minimum 12.5 mm. Potential evapotranspiration is increased during the summer months due to higher temperatures, higher radiation and advanced plant development. This can be observed in Figure 3.23 as an incline of ET_p in the beginning of the observed time interval for the cropped surface area. This effect is reversed later in the observed time period when, additionally to a reduction of ET_0, crops are either entering a senescence stage or are being harvested. Both events lower the potential evapotranspiration of the surface (also expressed in the lowering of K_c).

The total potential evapotranspiration calculated for the extent of the respective surface area is given in Table 3.9.

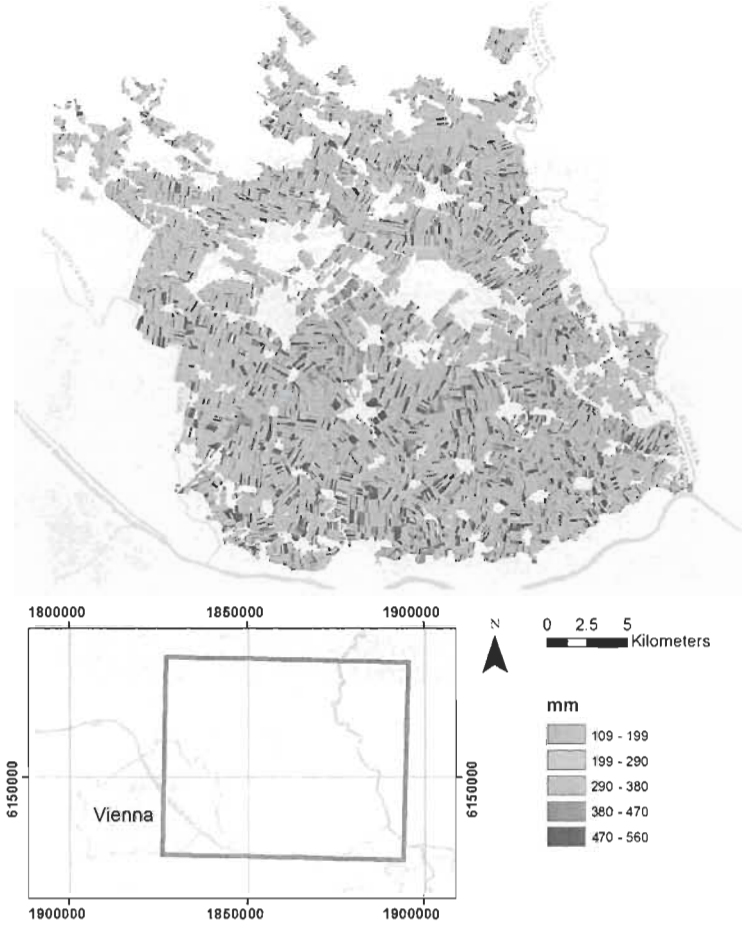

Figure 3.19: Seasonal potential evapotranspiration of the agricultural area in Marchfeld from June 10th to September 23rd

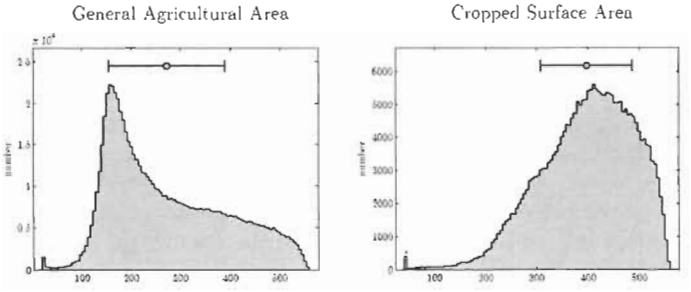

Figure 3.20: Histogram for the cumulated evapotranspiration raster-image (see Figure 3.19).

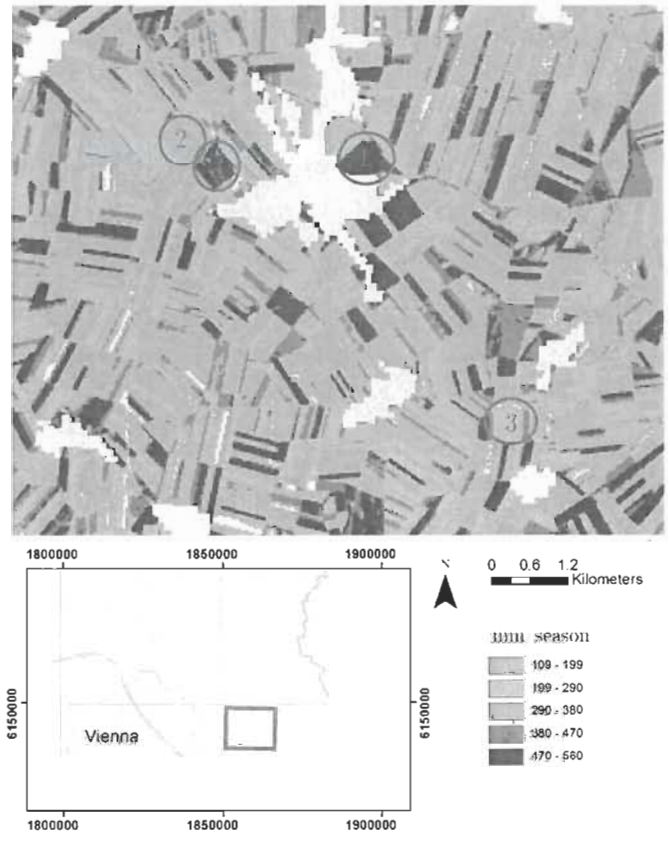

Figure 3.21: Location of sample points displayed in Figure 3.22

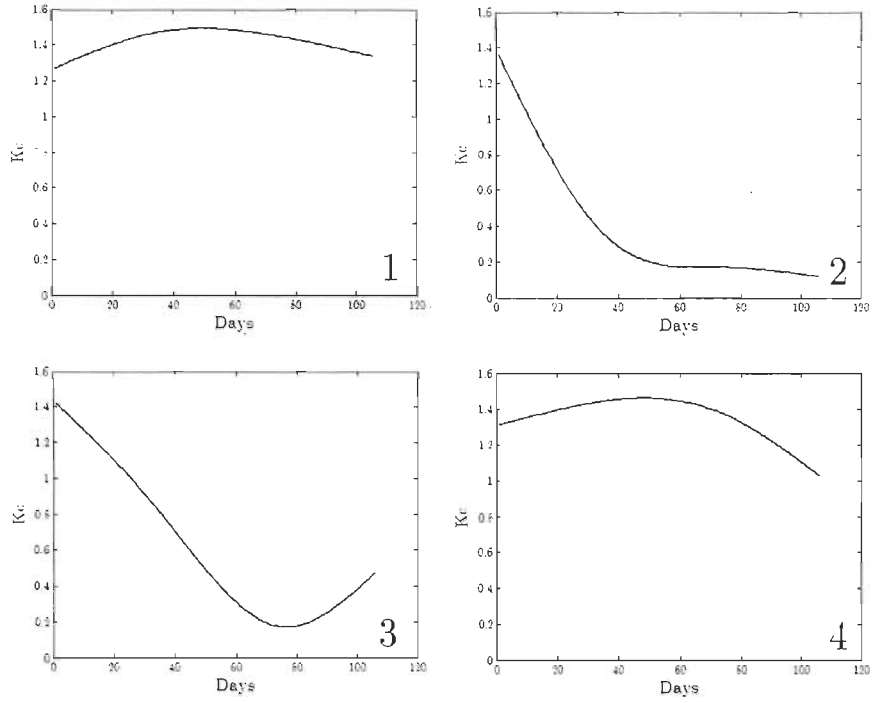

Figure 3.22: K_c developement over time from start of the image acquisition for four sample points indicated in Figure 3.21

Table 3.8: Estimated ET_p values over time for two surface estimations. General A. A. =General Agricultural Area. Date Format = M/DD

ETp [mm]	**6/10**	**6/20**	**6/30**	**7/10**	**7/20**	**7/30**	**8/9**	**8/19**	**8/29**	**9/8**
Cropped Surface	32.8	40.4	53.6	58.6	48.0	40.2	41.6	38.9	21.8	19.3
General A. A.	36.2	35.7	40.6	39.0	29.4	23.8	24.2	22.5	13.0	12.5

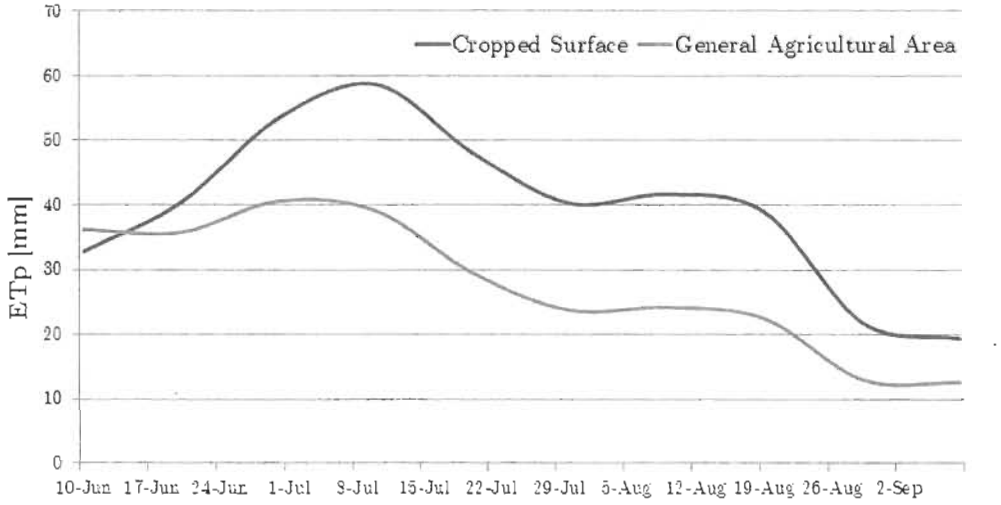

Figure 3.23: ET_p estimation for cropped surface area and the general agricultural area of the Marchfeld Region

Table 3.9: The total ET_p for the observed time frame of two area estimations

Surface Type	Total potential evapotranspiration
General Agricultural Area	174.29 Mio. m^3
Cropped Surface	86.09 Mio. m^3

3.4 Calculation of effective precipitation and water requirements

3.4.1 Calculation of effective precipitation

To account for a number of unknown factors like soil type, soil conditions, crop type, irrigation management etc. effective precipitation for the region was given as a range between a minimum and a maximum estimation. The estimations of effective precipitation cumulated to 10-day time intervals resulted in minimum of 0 (P_emin and P_emax) and maxima of $P_emin = 23.8$ and $P_emax = 39.5$. The maxima were observed in the beginning of the growing season following a sharp decrease in the following months. A second peak can be observed at the end of July where effective precipitation was estimated to be within a range of 23.7 to 39.5 mm (see Figure 3.24). With 759.5 mm annual precipitation was higher than the long-term average of 550 mm. An overview of the P_e-estimations is given in Table 3.10.

3.4.2 Calculation of water requirements

The estimation of water requirement was done for cumulated periods (10-day) and resulted in surplus values of +19.6 mm to a deficit of -50.4 mm. Water deficit is the highest from mid-June to beginning of July (-34.1 to -50.3 mm/10 days). During this time agricultural crop was well developed and meteorological conditions allowed for high evapotranspiration while precipitation was low. Towards the end of July the water deficit was lowered due to increasing precipitation and a decrease of potential evapotranpsiration of agricultural crops (harvest or senescence). Figure 3.25 plots the cumulated periods for the observed time frame.

The **total estimation of water deficit** for cropped surfaces in the agricultural region of Marchfeld from June 10th to September 23rd in the year 2010 ranges from **-32.02 to -52.8 Mio. m^3**.

Estimations of groundwater withdrawals for agricultural irrigation within the Marchfeld region were performed by the Marchfeldkanal Company. The estimations for the last 20 years vary between -9.8 to -45.1 Mio. m^3. These figures are a result of measurements of groundwater level fluctuations for representative test-sites. The Marchfeldkanal Company attempts to estimate the withdrawal for irrigation purposes by limiting the time frame to summer periods were distinct drops in the groundwater levels can be observed (in assumption that these drops are a result of irrigation practices). This way the irrigation season for the year 2010 was estimated to start on June 24th and to end on July 17th. The estimation of groundwater withdrawal for irrigation for this time period is 14.5 Mio. m^3.

For comparison the EO based estimation presented in this thesis was limited to the same time frame and resulted in a crop water requirement of 21.8 to 24.5 Mio m^3.

When comparing the two estimation it has to be taken into account that the calculation by the Marchfeldkanal-Company aims to represent actual *applied irrigation* whereas the calculation presented in this thesis aims to represent the *maximum water requirement of crops*. Furthermore presented method incorporated the cropped surface area in its full extent whereas irrigation infrastructure can be assumed to only cover a fraction of the same surface.

Table 3.10: Estimated values for precipitation, effective precipitation and the resulting water balance for each calculation of effective precipitation for the cropped surface area of Marchfeld in the year 2010 aggregated in 10 day time steps. Date format = M/DD

[mm]	6/10	6/20	6/30	7/10	7/20	7/30	8/9	8/19	8/29	9/8
Precipitation	70	1	9	33	47	53	46	23	36	13
$P_{e\,min}$	36	0	3	20	22	24	23	8	16	2
Water req.	3	-40	-50	-39	-26	-16	-19	-31	-6	-17
$P_{e\,max}$	52	1	7	24	35	39	35	17	27	10
Water req	20	-39	-47	-34	-13	-1	-7	-21	5	-9

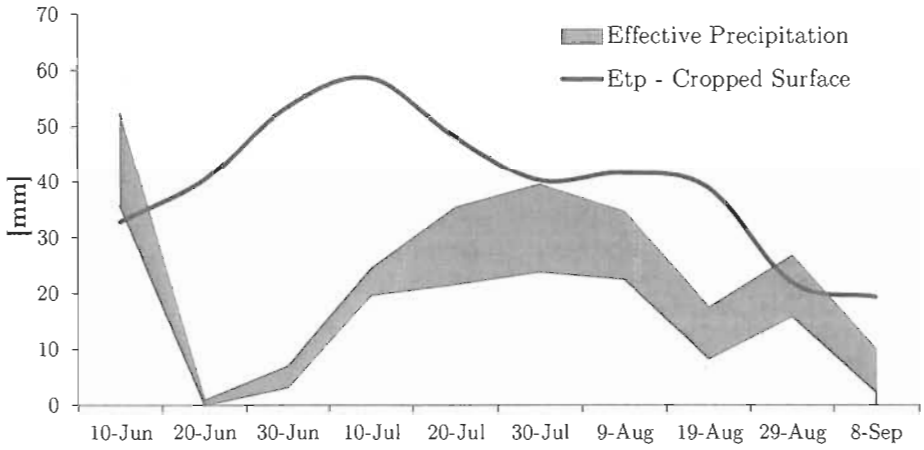

Figure 3.24: ET_p for the cropped surface area and effctive precipitation in the Marchfeld region for the irrigation season 2010

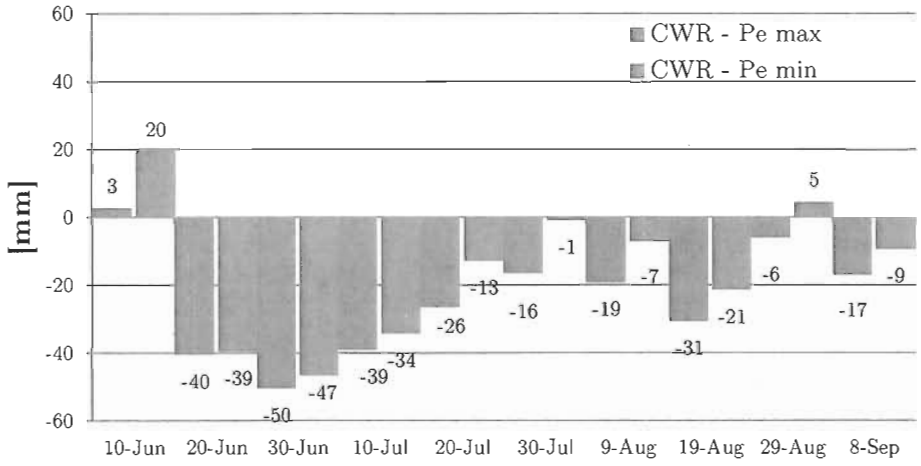

Figure 3.25: Water requirement of the cropped surface area in the Marchfeld region in the year 2010 aggregated in 10 days time-steps

Chapter 4

Conclusion

This thesis describes the estimation of water requirements in the context of agricultural production in the water-scarce environment of Marchfeld.

Reference evapotranspiration was calculated from meteorological data recorded at the ZAMG weather station in Zwerndorf by applying the FAO-56 Penman-Monteith equation. A time series of Landsat-5 observations was acquired for deriving information about the extent of the surface area for crops, the crop coefficient and the potential evapotranspiration. In a pre-processing step the EO dataset was atmospherically corrected with two software tools (FLAASH, ATCOR) and their performance was compared by analysis of pseudo-invariant targets. EO data was used for calculation of albedo (wavelength integrated ground reflectance) and LAI (through the CLAIR-model). A sensitivity analysis was performed to evaluate the influence of different parameters on the calculation of the crop coefficient. Meteorological and EO data were combined to calculate potential evapotranspiration. The EO dataset was further used in a classification to estimate the extent of the agricultural surface area. A range of plant effective precipitation was calculated from meteorological data. The water requirement for the region during the observed time period was then calculated.

The highest potential evapotranspiration for the full observed time period from June 10th to September 23rd was 560 mm. The total estimated water requirement ranged from 32.02 to 52.8 Mio. m^3. The observed peak of water deficit (5 mm/day) was observed at the end of June.

Further improvement of the methodology can be achieved at the step of atmospheric correction and assessment of effective precipitation. For the former; accompanying measurements for model input and reference could help to improve the performance. For the latter; the variation of soil types and their storage capacity must be incorporated. The Marchfeld-Region has a great variation of soil-types; implementation of this aspect is of particular importance when working on field scale since soil conditions and thus water requirements will vary from field to field. A prerequisite for this is the availability of data on soil types and soil conditions.

The type of information generated with this methodology can be used at field or regional scale. It generates information about the crop surface in a temporal and spatial dimension. Providing precise information about the observed region can help managers at regional scale and farmers in their decision making progress. Regions of high water demand can be identified and allocation of resources properly managed. A critical factor for agricultural production is the high water deficit at the start of the growing season. If not managed properly this circumstance could lead to water stress and further effect plant vigour and ultimately yield stability. In an extended context the data on crop development itself (e.g.: LAI, K_c) can be used as additional source of information. This data can be used to compare different fields, soil types, seed types, management practices and vegetation periods to one another. EO-data of agricultural regions

can also be used in applications other than estimation of water requirements such as biomass-, yield estimation, cropland mapping and others.

For improvement of agricultural management practices this data has to be relayed to farmer level in an accessible and user friendly way. Moreover the information needs to be provided in a timely matter for the farmer to react duly on possible stress conditions.

Appendix A

Publication

Remote Sens. **2013**, *5*, 1274-1291; doi:10.3390/rs5031274

OPEN ACCESS

Remote Sensing

ISSN 2072-4292

www.mdpi.com/journal/remotesensing

Article

Estimation of Leaf Area Index Using DEIMOS-1 Data: Application and Transferability of a Semi-Empirical Relationship between two Agricultural Areas

Francesco Vuolo [1,*], Nikolaus Neugebauer [1], Salvatore Falanga Bolognesi [2], Clement Atzberger [1] and Guido D'Urso [3]

[1] Institute of Surveying, Remote Sensing and Land Information (IVFL), University of Natural Resources and Life Sciences (BOKU), Peter Jordan Str. 82, A-1190 Vienna, Austria; E-Mails: Nikolaus.Neugebauer@boku.ac.at (N.N.); clement.atzberger@boku.ac.at (C.A.)

[2] Ariespace s.r.l., Centro Direzionale Is. A3, I-80143 Napoli, Italy; E-Mail: salvatore.falanga@ariespace.com

[3] Department of Agricultural Engineering and Agronomy, University of Naples Federico II, Via Università 100, I-80055 Portici, Italy; E-Mail: durso@unina.it

* Author to whom correspondence should be addressed; E-Mail: francesco.vuolo@boku.ac.at; Tel.: +43-1-47654-5135; Fax: +43-1-47654-5142.

Received: 16 January 2013; in revised form: 6 March 2013 / Accepted: 6 March 2013 / Published: 12 March 2013

Abstract: This work evaluates different procedures for the application of a semi-empirical model to derive time-series of Leaf Area Index (LAI) maps in operation frameworks. For demonstration, multi-temporal observations of DEIMOS-1 satellite sensor data were used. The datasets were acquired during the 2012 growing season over two agricultural regions in Southern Italy and Eastern Austria (eight and five multi-temporal acquisitions, respectively). Contemporaneous field estimates of LAI (74 and 55 measurements, respectively) were collected using an indirect method (LAI-2000) over a range of LAI values and crop types. The atmospherically corrected reflectance in red and near-infrared spectral bands was used to calculate the Weighted Difference Vegetation Index (WDVI) and to establish a relationship between LAI and WDVI based on the CLAIR model. Bootstrapping approaches were used to validate the models and to calculate the Root Mean Square Error (RMSE) and the coefficient of determination (R^2) between measured and predicted LAI, as well as corresponding confidence intervals. The most suitable approach, which at the same time had the minimum requirements for fieldwork, resulted in a RMSE of 0.407 and R^2 of 0.88 for Italy and a RMSE of 0.86 and R^2 of 0.64 for the Austrian test site. Considering

this procedure, we also evaluated the transferability of the local CLAIR model parameters between the two test sites observing no significant decrease in estimation accuracies. Additionally, we investigated two other statistical methods to estimate LAI based on: (a) Support Vector Machine (SVM) and (b) Random Forest (RF) regressions. Though the accuracy was comparable to the CLAIR model for each test site, we observed severe limitations in the transferability of these statistical methods between test sites with an increase in RMSE up to 24.5% for RF and 38.9% for SVM.

Keywords: LAI; DEIMOS; satellite time-series; calibration; WDVI; Random Forest; Support Vector Machine; regression

1. Introduction

In the recent years, the use of satellite sensor data has become more common in precision agriculture technologies [1], and various operational services are being developed within the Global Monitoring for Environment and Security (GMES) initiative [2]. In this context, the data users (*i.e.*, farmers, large and small scale agri-businesses) are mostly interested in monitoring the spatial distribution of some crop characteristics over the growing season and time-series of satellite acquisitions at high spatial resolution are a major source of information.

A key vegetation parameter attracting most interest is the Leaf Area Index (LAI), defined as the total one-sided area of green leaf area per unit ground surface area [3]. LAI is used to derive agronomical indicators for various crop management purposes. For instance, LAI maps are used in agro-meteorological models to derive the crop water needs (an example of operative application is given in *Irrisat*) [4], to monitor the nitrogen status and to apply fertilizer with variable rates (e.g., *FarmSat*), as input in crop models to derive agronomical variables [5,6]. On a larger scale, LAI and other biophysical variables are used for example for yield predictions at administrative level [7–9]. A general overview of remote sensing contributions to agriculture is given in [10].

Two groups of techniques have been commonly applied for the estimation of the LAI from optical satellite sensor data using semi-empirical/statistical approaches (*i.e.*, vegetation indices, VI) or physical based approaches of leaf-canopy radiative transfer model (RTM) inversion [11,12]. Most of the empirical or statistical equations, such as regressions between spectral reflectance, vegetation indices (VI) or shape indices (e.g., red edge) and field measurements [13–15], employ data in two or more wavebands, usually red and near-infrared [16,17]. VIs are often the only option for the retrieval of LAI with limited spectral information (such as in the case of DEIMOS-1 data with only three spectral bands).

A prerequisite for the quantitative analysis of time-series of satellite sensor data is to perform radiometric and atmospheric corrections [18], if possible using reliable instantaneous atmospheric measurements (such as aerosol optical thickness, water vapor content) and/or the spectral reflectance of known ground targets either derived from ground measurements (surface and/or atmospheric conditions) or from consolidated library data [19,20]. Several approaches have been proposed for performing atmospheric corrections. An operative procedure is based on the use of look-up-tables (LUT) with pre-calculated atmospheric RTM simulations for different satellite sensor types [20,21]. However,

model assumptions and simplifications often lead to inaccuracies in the estimated top-of-canopy (TOC) reflectance measurements [22].

The inherent inaccuracy of TOC reflectance data can be accounted for by using image-specific calibration procedures to estimate LAI. A typical example is the use of soil line-based VIs in place of intrinsic VIs [23]: in this case the image-specific tuning of the soil line slope parameter can be used to increase the consistency in the analysis of atmospherically corrected products, especially for time-series datasets.

In this study, the application of image-specific calibration procedures to estimate LAI was tested. We used satellite time-series from DEIMOS-1 data, an operational satellite in the DMC constellation, acquiring radiance in three spectral bands (green, red and near-infrared) at 22 m spatial resolution. DEIMOS-1 satellite is equipped with a wide-image-swath sensor (630 km), providing a large coverage and overlap between scenes and therefore increasing the revisit time and the probability of capturing cloud-free images. Considering the available spectral resolution of the sensor, we selected a simple LAI retrieval approach based on a VI using the CLAIR model [24]. This approach has been tested using canopy reflectance model data [24], field-based reflectance measurements [25] and satellite data in a number of studies [4,26].

The main goal of this work was to evaluate different operational strategies to identify the parameters of the semi-empirical CLAIR model to estimate LAI. Within this main goal, we assessed the transferability of the model parameters between test sites. For comparison, two relatively novel statistical methods were also investigated using Random Forest (RF) and Support Vector Machine (SVM) regressions.

In addressing these issues, the study provides recommendations for deriving consistent time-series maps of LAI in operational frameworks at moderate (22 m) spatial resolution with limited spectral information. Other statistical LAI mapping approaches are presented in other papers of this special issue [27].

2. Materials and Methods

2.1. Overview

The described methodology provides an operational perspective to identify the parameters of the semi-empirical CLAIR model [24,28] for deriving consistent time-series LAI maps. A set of DEIMOS-1 satellite sensor data were acquired over two agricultural regions in Southern Italy and Eastern Austria during one growing season. Contemporaneous field estimates of LAI were collected for a number of fields and crops. Using this dataset, three operational procedures were tested (Table 1). First, we considered a test site specific application based on seasonal average (constant) values of the CLAIR model parameters, namely the soil line slope, the $WDVI_\infty$ (representing the asymptotically limiting value for the Weighted Difference Vegetation Index (WDVI) when LAI tends to infinity) and the α extinction and scattering coefficient. Secondly, we derived the model parameters for each satellite acquisition separately. Finally, we tested an intermediate solution based on an image-specific estimation of the parameters that can be extracted directly from the images (*i.e.*, soil line slope and $WDVI_\infty$) and on a seasonal average (constant) value of the parameter that requires contemporaneous

field measurements (*i.e.*, the α coefficient). Additionally, we evaluated the transferability of local models between the two test sites. For comparison, two other statistical methods to estimate LAI were also investigated: Random Forest (RF) and Support Vector Machine (SVM) regressions.

Table 1. Summary of the three procedures to derive the CLAIR model parameters. The 'soil line slope' represents the slope of the linear relationship between red and near-infrared reflectance of bare soil pixels. The $WDVI_{\infty}$ is the asymptotically limiting value for the Weighted Difference Vegetation Index (WDVI) when LAI tends to infinity and α is the extinction and scattering coefficient of the CLAIR model. A fourth procedure consisted in transferring the model parameters from one test site to another.

Procedures	Soil Line Slope	$WDVI_{\infty}$	α
1	constant	Constant	constant
2	image-specific	image-specific	image-specific
3	image-specific	image-specific	constant
Transferability	image-specific	image-specific	constant

2.2. Field Experimental Campaigns

The field and satellite data used in this study were acquired in the context of two field campaigns carried out in two agricultural regions located in Southern Italy and in Eastern Austria during the 2012 growing season. The Italian field campaign was undertaken at the 500 km^2 '*Piana del Sele*' and at the 3820 km^2 '*Piana del Volturno*' sites in the Campania region of Southern Italy (Figure 1) (Lat. 40.52°N, Long. 15.00°E). The two sites are large agricultural regions and are characterized by irrigated agriculture (mainly forage crops, fruit trees and vegetables) with an average field size of about 2 ha [29]. The first site is characterized by very different soil types including Mollisols, Alfisols, Inceptisols and Entisols [30] according to the United States Department of Agriculture (USDA) soil taxonomy; the second plain is an alluvial formation with soil types varying from Entisols to Vertisols [31]. The average annual precipitation is about 800 mm, mostly concentrated during the winter months, with dry and warm summers. Maximum reference evapotranspiration rates, generally occurring during the second half of July, range between 3 and 5 mm/d [32].

The Austrian field campaign was undertaken at the 1000 km^2 '*Marchfeld region*' in Lower Austria (Lat. 48.20°N, Long. 16.72°E). The dominant soil types are Chernozem and Fluvisol, based on the Food and Agriculture Organization (FAO) World Soil Classification. The general soil conditions are characterized by a humus-rich A horizon and a sandy C horizon, followed by fluvial gravel from the former river bed of the Danube [33]. The region is characterized by a semi-arid climate with an average annual precipitation of 500–550 mm that can drop to 300 mm making it the driest region of Austria. Precipitation during the growing season (April–September) is 200–440 mm. Irrigation in Lower Austria has made it possible to establish a variety of crops thus contributing to the importance of Marchfeld in agricultural production. About 65000 ha of the area in Marchfeld are used for agricultural production. The main crops are vegetables (11%), sugarbeet (10%) and potatoes (7%).

Within these two large and relatively flat regions, LAI was estimated within 400 m^2 elementary sampling units (ESU) that were relatively homogeneous in terms of both vegetation type and growth stage. The center of each ESU was geo-located by means of a GPS, with an accuracy of ±3–5 m.

Figure 1. Selected study regions. The study was carried out in an agricultural region located in the Eastern part of Austria ('*Marchfeld region*') and in two areas ('*Piana del Sele*' and '*Piana del Volturno*') located in the Campania region in Southern Italy.

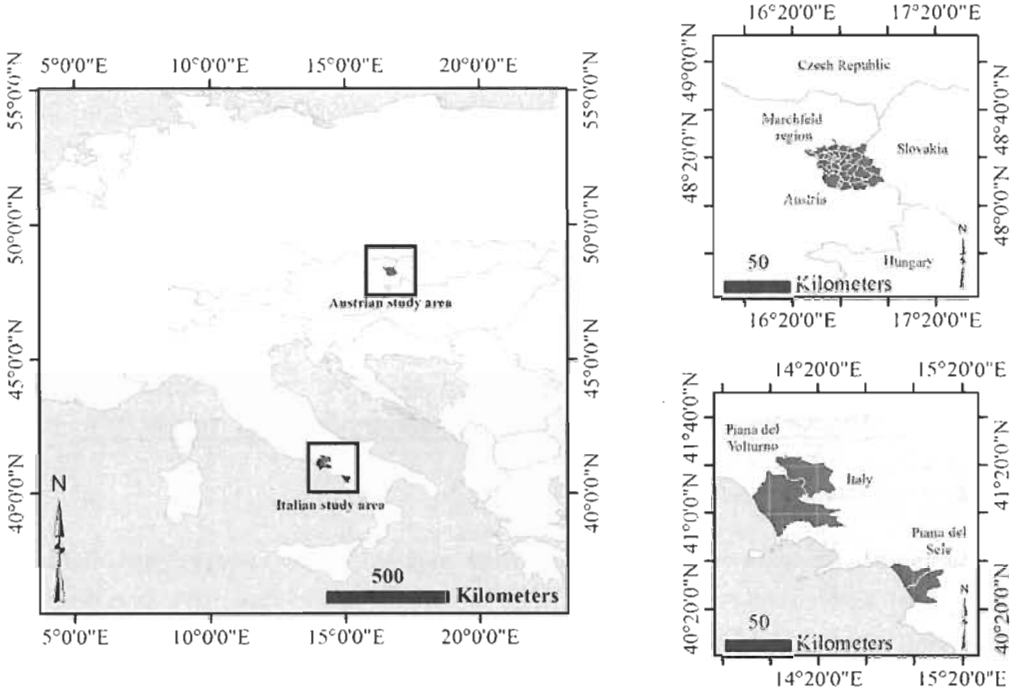

For the Italian case study, LAI was sampled within ESUs over a period of three months (July–September 2012) in correspondence of each satellite acquisition for a total of 74 multi-temporal measurements comprising 11 ESUs (5 alfalfa and 6 maize fields in '*Piana del Sele*') and 8 ESUs (3 alfalfa and 5 maize fields in '*Piana del Volturno*'). LAI values within the 19 ESUs ranged between 0.2 and 4.9 with a mean of 2.4 and a standard deviation of 1.2.

LAI in the '*Marchfeld region*' was sampled within 55 ESUs for a range of crops including maize (10 ESUs), sugarbeet (7 ESUs), vineyards (7 ESUs), carrots (5 ESUs) and other crops (26 ESUs). LAI values within the 55 ESUs ranged between 0.1 and 5.8 with a mean of 2.2 and a standard deviation of 1.36. A summary of the field and satellite data acquisitions is given in Table 2.

LAI was estimated using the Plant Canopy Analyzer LAI-2000 [34]. Measurements were made during early morning and late afternoon under diffuse light conditions to minimize the effects of direct sunlight otherwise leading to LAI underestimation [35]. A view cap of 180 degrees was used to physically limit the sensor field-of-view and thus to reduce interference due to the presence of an operator. There are some limitations in this type of indirect measurements technique [36]. On the one hand, the LAI-2000 sensor does not distinguish photosynthetically active leaf tissue from other plant elements, such as stems, flowers or senescent leaves. This leads to overestimated LAI. On the other hand, the 'clumping effect', *i.e.*, non-random positioning of canopy elements, is also neglected by the measurement device causing LAI underestimation. Hence, some compensation can be assumed [37]. The LAI recorded using the LAI-2000 sensor represents a measure close to the effective Plant Area Index ('PAIe') for reasons discussed above [37]. The average LAI, resulting from three replications of

one above-canopy and nine below-canopy measurements, was taken as representative measure for each ESU. The three replications (for a total of 27 measurements) were sampled randomly within the ESU. The same sampling protocol was used in Austria and in Italy and throughout the three months field campaigns.

Table 2. Timing of the field campaigns and satellite acquisitions with corresponding statistics of the LAI measurements. Note that acquisitions were not always performed during the same dates in the two areas (*Sele* and *Volturno*) of the Italian test site.

Field Campaign Dates	Satellite Acquisition Dates	No. of Samples	LAI		
			Min	Max	Mean
Italy	*(Sele // Volturno)*				
04/07	04/07 // 07/07	11	0.20	3.32	1.32
11/07	10/07 // 13/07	12	0.25	3.77	1.78
17/07	20/07 // 20/07	12	0.39	4.62	2.36
26/07	29/07	12	0.44	4.08	2.72
31/07	05/08	7	1.63	3.39	2.95
07/08	11/08	7	0.63	4.13	2.95
13/08	18/08	10	0.74	4.92	3.16
10/09	09/09	3	2.43	2.84	2.68
Austria	*(Marchfeld)*				
04/07		9	0.44	4.48	2.18
02/08		20	0.11	4.52	1.75
22/08	Coincident with field campaigns	10	0.15	3.31	1.82
07/09		6	1.79	5.79	2.83
21/09		10	0.93	5.10	2.96

2.3. Satellite Data

Multispectral data were acquired from DEIMOS-1, a satellite in the DMC constellation. The sensor records radiance in three broad spectral bands corresponding to green, red, and near-infrared parts of the electromagnetic spectrum at a ground sampling distance (GSD) of 22 m. Five and eight scenes were acquired during the 2012 growing season (Table 2) for the Austrian and for the Italian case studies, respectively. Satellite images were provided orthorectified to sub-pixel accuracy (~10 m) using ground control points and the Shuttle Radar Topography Mission (SRTM v3) data as digital elevation model. The image data were atmospherically corrected by using ATCOR-2 [20]. For the Austrian test site, during the image acquisition campaign, five reference measurements of ground spectral reflectance (bare soils, dry and dense vegetation) were taken in correspondence of one satellite acquisition (August 2nd). A subset of these measurements was used to perform the atmospheric correction. The other subset was used to validate the results of the correction algorithm. The atmospheric correction for the other images in the time-series was cross-checked by observation of pseudo-invariant targets within the study area [19]. A similar procedure was used for the Italian test site and the accuracy of the atmospheric correction was checked against a set of reference pixels containing identifiable pseudo-invariant ground targets (*i.e.*, asphalt, sea water, concrete and sand) with known reflectance values from a spectral library [20].

Figure 2. An example of the time-series of DEIMOS-1 satellite sensor data for an area in the Marchfeld region (Austria). Five images were acquired to monitor the crop development during the growing season (June–September). The images were atmospherically corrected using ATCOR-2. RGB composites correspond to Near-infrared, Red and Green channels.

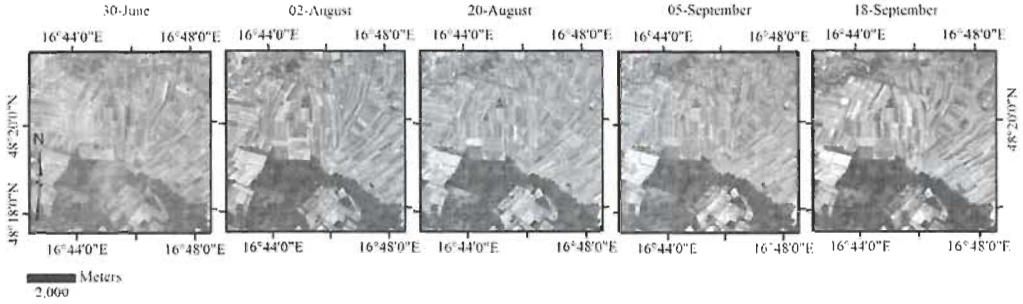

2.4. Estimation of Leaf Area Index

In this study, we selected a simple semi-empirical model and two statistical methods to estimate LAI. In all cases, we used the TOC (atmospherically corrected) reflectance data. Regarding the semi-empirical model, two spectral bands (red and near-infrared) were used to calculate the Weighted Difference Vegetation Index (WDVI), which was related to LAI through an inverse exponential relationship using the CLAIR model [24,28]. Regarding the statistical methods two models were applied: the first based on a regression tree algorithm using Random Forest (RF) and the second based on a linear kernel Support Vector Machine (SVM) regression.

2.4.1. Semi-Empirical Estimation of LAI with the CLAIR Model

The CLAIR model is based on an inverse exponential relationship between LAI and the WDVI, which was derived using field spectral radiometer data experimentally [24,28]. This relationship is built upon a simplified reflectance model of the light extinction through the vegetation canopy. The WDVI is calculated from the reflectance in red (ρ_{red}) and near-infrared (ρ_{nir}) as follows:

$$\mathrm{WDVI} = \rho_{\mathrm{nir}} - \rho_{\mathrm{red}} * \frac{\rho_{s\,nir}}{\rho_{s\,red}} \quad (1)$$

where $\rho_{s\,nir}/\rho_{s\,red}$ represents the 'soil line slope', a linear relationship between red and near-infrared reflectance of bare soils [38]. The soil line slope parameter accounts for the effects of the soil background on the calculation of the vegetation index and it has to be determined for each test site [23]. Based on the WDVI, LAI is determined according to the following equation [28]:

$$\mathrm{LAI} = -\frac{1}{\alpha} * \ln\left(1 - \frac{\mathrm{WDVI}}{\mathrm{WDVI}_{\infty}}\right) \quad (2)$$

where α is an extinction and scattering coefficient and WDVI_{∞} is the asymptotically limiting value for the WDVI. The two model parameters (WDVI_{∞} and the α coefficient) can be estimated empirically using a set of LAI values from field measurements and contemporaneous reflectance values from satellite sensor data [24]. Generally, WDVI_{∞} is derived directly from the image data considering the maximum WDVI value for vegetated areas in correspondence of saturation (LAI < 6). The α

coefficient can be calibrated using a regression analysis technique applied to observed and estimated LAI values [4]. This latter parameter describes the canopy architecture and it is dependent on the crop type and the corresponding Leaf Angle Distribution (LAD) value.

Different values of the parameters in Equation (2) can be found in the literature. For instance, Clevers [25] reported an α value ranging between 0.252 and 0.53 and $WDVI_\infty$ ranging between 68.6 and 57.9 for vegetative and generative growth stages of barley respectively.

In this study, we visually selected about 40–60 sample points of bare soils within each of the acquired satellite image data and the reflectance of these points was used for calculation of the soil line slope. The soil line slope was then used to calculate the WDVI. The $WDVI_\infty$ value was extracted for each image. Then, we derived the α coefficient using an unconstrained nonlinear optimization method, which minimizes the Root Mean Square Error (RMSE) (our cost function) between measurements and predictions of LAI values. An initial α value of 0.35 was used as first guess based on previous campaigns for the Italian test site. We checked different starting values, which always converged at the same final result.

We tested three different procedures (Table 1) to derive a set of α and $WDVI_\infty$ values to be applied throughout the growing season. Firstly we considered a test site specific estimation of the empirical parameters of Equations (1) and (2) obtaining one seasonal average (constant) value of the soil line slope and of $WDVI_\infty$. The α coefficient was derived using the pooled set of LAI measurements acquired during the three months campaign. In this way, the time-series field and satellite datasets were considered as a unique dataset. This procedure was repeated independently for each of the two test sites under investigation. In this case, we would perform field measurements for each new test site only during the first year or during short field campaigns before the operational activities. Once calibrated, the model parameters could be applied to the newly acquired images, without further need for field work.

The second procedure consisted in deriving a set of image-specific model parameters for each new satellite acquisition. In this case, we calibrated the α coefficient using only the LAI measurements acquired in correspondence of each acquisition. To avoid introducing biases related to measurements taken on different dates, we did not consider antecedent measurements. This procedure represents the most intensive and time consuming approach, in which we would need field campaigns for each new satellite overpass for the estimation of image-specific α coefficients. Similarly, we would extract a certain number of points from each image in order to calculate the soil line slope and the $WDVI_\infty$.

Differently, a constant α value to be applied throughout the growing season for each test site was considered as third procedure. This represents an intermediate solution in terms of resources required since we retain the same approach of the second case for deriving image-specific soil line slope and $WDVI_\infty$ values.

These three procedures reflect possible practical approaches for applying the CLAIR model in order to derive time-series of LAI maps in nearly real-time (48 h from satellite acquisitions) and for operational campaigns. For instance, the CLAIR model has been used to derive LAI for the calculation of crop water requirements in irrigation advisory services [4].

Considering the feasible size of the field datasets for this kind of analysis (74 and 55 measurements for Italy and Austria, respectively), the validation of the model performance was achieved by resampling the field dataset using a bootstrapping approach with 200 repetitions [39] in order to

provide an unbiased estimation of the model accuracy [40]. To quantify the model prediction accuracies we used the following statistical measures: RMSE, the coefficient of determination (R^2) between measured and predicted LAI and the confidence intervals.

2.4.2. Statistical Based Approaches for the Estimation of LAI: Support Vector Machine (SVM) and Random Forest (RF) Regression

A second group of techniques were applied for the estimation of LAI based on statistical models established using (1) a least-squares version of a support vector machine (SVM) regression and (2) a regression tree using Random Forest (RF) algorithm.

SVMs have been developed in the framework of statistical learning theory by Vapnik [41] for classification purposes and have been recently extended to regression problems [42]. SVMs have been applied for the estimation of LAI in previous studies [43–46] providing satisfactory results. A comprehensive tutorial for SVM regression was provided by [47]. In this study we used a SVM implemented by [48] as a Matlab toolbox. We selected a linear kernel function, which provided better results compared to polynomial or radial basis functions.

RF is an ensemble algorithm developed by Breiman [49]. It consists of several regression trees; each tree is trained on a bootstrap sample of the training dataset and the majority vote is taken for the RF prediction. Random subsets of input variables are used to train the regression tree. The algorithm provides an internal unbiased estimate of the error using the so-called 'out-of-bag' (OOB) samples. RF has been successfully used in several classification problems but limited application to biophysical vegetation parameters retrieval can be found in the literature [50,51]. In this study we used a Matlab implementation of RF [52] with a default set of model parameters (no. of trees = 500; no. of input variables randomly chosen at each split = 2).

For both SVM and RF, the regressions were established using LAI measurements and atmospherically corrected reflectance values in green, red and near-infrared bands. Additionally, date-specific WDVI and $WDVI_\infty$ values were used as input variables. This set of variables provided the most stable and accurate results compared to using seasonal average of WDVI and $WDVI_\infty$ values or reflectance only. In the case of SVM, we first optimized the regularization parameter γ of SVM model using a simplex search method and a leave-one-out cross validation approach with the experimental LAI dataset. Then, two models (one for each test site) were applied to the experimental datasets to calculate RMSE and R^2. In the case of RF, the model performance was calculated using the RMSE obtained from the average OOB Mean Square Error (MSE) over 500 trees. A pseudo-coefficient of determination (pseudo-R^2) was calculated as follows: 1 − MSE/variance (LAI).

3. Results and Discussion

3.1. Identification of the CLAIR Model Parameters and LAI Estimation Accuracy

Procedure 1: the soil line slope and of the asymptotic limiting value for the WDVI ($WDVI_\infty$), along with the dates for field campaigns and satellite acquisitions are presented in Table 3. The α coefficient was derived using a bootstrap approach with 200 resampling of the experimental LAI dataset. The RMSE and R^2 between measured and predicted LAI and the corresponding α coefficient were taken as

the median values of the 200 bootstrap estimations. Prediction accuracies are presented in Table 4. The scatterplots between field and satellite estimates of LAI are shown in Figure 3. Applying this first procedure resulted in a RMSE of 0.817 and a R^2 of 0.57 for the study region in Italy. For Austria, the RMSE was 1.037 and R^2 was 0.57. It can be observed that the distance from the 1:1 line increases with higher values of both measured and estimated LAI. In addition, the variation of the actual estimates increases along with the LAI-value, an effect which was greatly reduced for the study region in Italy by using the second procedure. As expected, the RMSE for the Austrian case study was higher given the larger variability of the crop types in this area compared to Italy.

Procedure 2: the LAI measurements from the last two field campaigns (31/07 and 07/08, 13/08 and 10/09) and the corresponding image data for the Italian test site were combined in a single dataset due to a limited number of field measurements. Similarly, the LAI and image data from the last campaign (07/09 and 21/09) for the Austria test site were combined. The number of LAI measurements used for each image-specific calibration, including LAI statistics (minimum, maximum and mean values) is provided in Table 2.

The scatterplots between field and satellite estimates of LAI are shown in Figure 4. Varying the soil line slope and thus WDVI values helped to improve WDVI based LAI estimation. Using the parameters (soil line slope and $WDVI_\infty$) listed in Table 3 resulted in an RMSE of 0.388 and R^2 of 0.89 for the test site in Italy (Table 4). In addition, the higher variation of LAI estimation could be reduced when compared to the first procedure. For the Austrian test site the RMSE was 0.82 and R^2 was 0.66. Analyzing the data presented in Table 4, we noticed that the range of variability of the α values (0.08) in the Austria test site is greater than the Italian one (0.04). This explains the larger RMSE observed in Austria as a consequence of the large crop variability in this area. In spite of this, larger errors are observed only for LAI values greater than 3.

Procedure 3: results are presented in Table 4 and in Figure 5. A constant α coefficient value throughout the growing seasons and image-specific variation of soil line slope and $WDVI_\infty$ resulted in a RMSE of 0.407 and R^2 of 0.88 for Italy and a RMSE of 0.86 and R^2 of 0.64 for the Austrian test site. No substantial changes in the performance of the LAI estimation were observed when comparing this procedure to the full image-specific procedure. The slight increase in the RMSE is compensated by the reduced field work requirements of this approach.

3.2. Parameterization of Support Vector Machine and Random Forest (RF) Regressions and LAI Estimation Accuracy

The results of the SVM tuning provided a γ value of 0.5435 and 0.2998 for Italy and Austria, respectively. The application of tuned models (one for each test site) to the experimental datasets resulted in a RMSE of 0.394 and 0.785 for the Italian and for the Austria test sites, respectively. R^2 resulted in 0.86 for Italy and 0.69 for Austria. The application of the RF regression achieved a RMSE (OOB) of 0.502 ± 0.027 and R^2 of 0.82 for the Italian case study and a RMSE of 0.860 ± 0.017 and R^2 of 0.63 for the Austrian case study. Compared to the CLAIR model performance, SVM achieved comparable accuracy for procedures 2 (Figure 4) and 3 (Figure 5) with image-specific soil line slope and $WDVI_\infty$ values. On the contrary, RF reported slightly lower accuracies for the Italian case study.

However, the error estimates obtained from the OOB samples might be more realistic compared to the RMSE estimates for SVM.

Table 3. Soil line slope and $WDVI_\infty$ values for each satellite image in the two study regions. The seasonal averages correspond to the constant values used in procedure 1. Image-specific soil line slope and $WDVI_\infty$ values were used for procedure 2 and 3.

	EO Acquisition Dates	Soil Line Slope	$WDVI_\infty$
Italy	*(Sele // Volturno)*		
Seasonal average		**1.35**	**0.518**
Seasonal Min-Max		**1.24–1.42**	**0.469–0.588**
Image 1	04/07 // 07/07	1.37 // 1.33	0.493 // 0.488
Image 2	10/07 // 13/07	1.38 // 1.32	0.50 // 0.495
Image 3	20/07 // 20/07	1.37 // 1.42	0.469 // 0.538
Image 4	29/07	1.33 // 1.37	0.56
Image 5	05/08	1.33 // 1.38	0.485
Image 6	11/08	1.24 / 1.38	0.588
Image 7	18/08	1.30 // 1.38	0.48 // 0.525
Image 8	09/09	1.31	0.54
Austria	*(Marchfeld)*		
Seasonal average		**1.47**	**0.596**
Seasonal Min-Max		**1.41–1.64**	**0.57–0.61**
Image 1	04/07	1.64	0.57
Image 2	02/08	1.41	0.61
Image 3	22/08	1.47	0.60
Image 4	07/09	1.43	0.60
Image 5	21/09	1.41	0.60

Table 4. Statistics of the CLAIR model accuracy based on the experimental field dataset.

Procedure	Case Study	Dataset	RMSE	R^2	α
1	**Italy**	*Combined image 1–8*	0.82 ± 0.01	0.58	**0.32** ± 0.01
	Austria	*Combined image 1–5*	1.04 ± 0.03	0.58	**0.39** ± 0.02
2	**Italy**	*Image 1*	0.23 ± 0.02	0.95	**0.34** ± 0.02
		Image 2	0.24 ± 0.01	0.96	**0.35** ± 0.01
		Image 3	0.24 ± 0.01	0.97	**0.37** ± 0.01
		Image 4	0.49 ± 0.03	0.75	**0.34** ± 0.02
		Image 5 & Image 6	0.44 ± 0.02	0.74	**0.33** ± 0.01
		Image 7 & Image 8	0.54 ± 0.03	0.82	**0.36** ± 0.02
	Austria	*Image 1*	0.79 ± 0.05	0.66	**0.32** ± 0.03
		Image 2	0.85 ± 0.03	0.64	**0.40** ± 0.04
		Image 3	0.53 ± 0.04	0.78	**0.32** ± 0.02
		Image 4 & Image 5	0.97 ± 0.04	0.54	**0.32** ± 0.02
3	**Italy**	*Combined image 1–8*	0.41 ± 0.004	0.88	**0.35** ± 0.01
	Austria	*Combined image 1–5*	0.86 ± 0.01	0.64	**0.34** ± 0.02

Figure 3. Procedure 1: scatterplots of the LAI estimation for the Italian case study (**a**) and for the Austria case study (**b**). Vertical error bars correspond to the Standard Error on LAI (SEL) measurements for each ESU. Horizontal error bars correspond to the Standard Error on LAI predictions and it was estimated using resampling with 200 bootstraps.

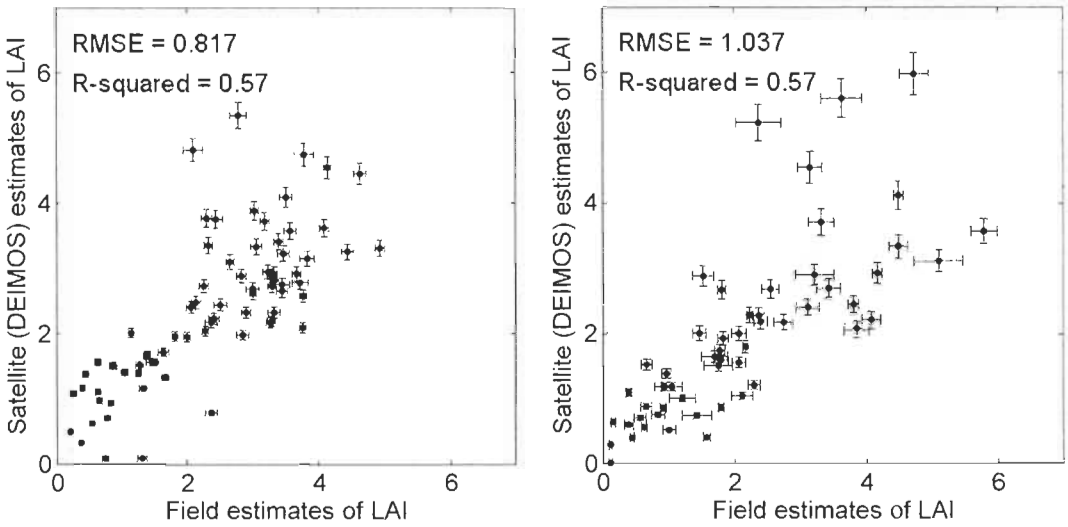

Figure 4. Procedure 2: scatterplots of the LAI estimation for the Italian case study (**a**) and for the Austria case study (**b**).

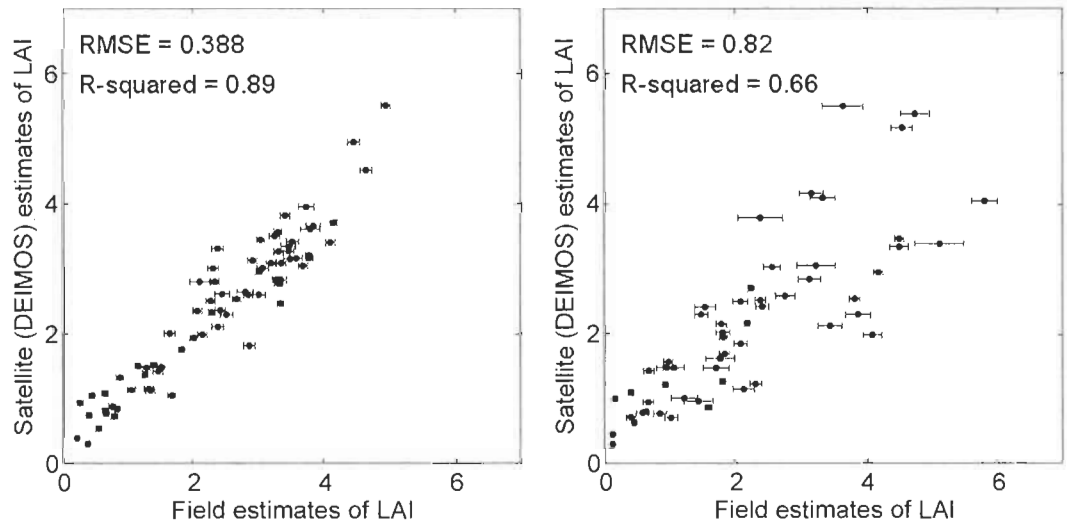

Figure 5. Procedure 3: scatterplots of the LAI estimation for the Italian case study (**a**) and for the Austria case study (**b**).

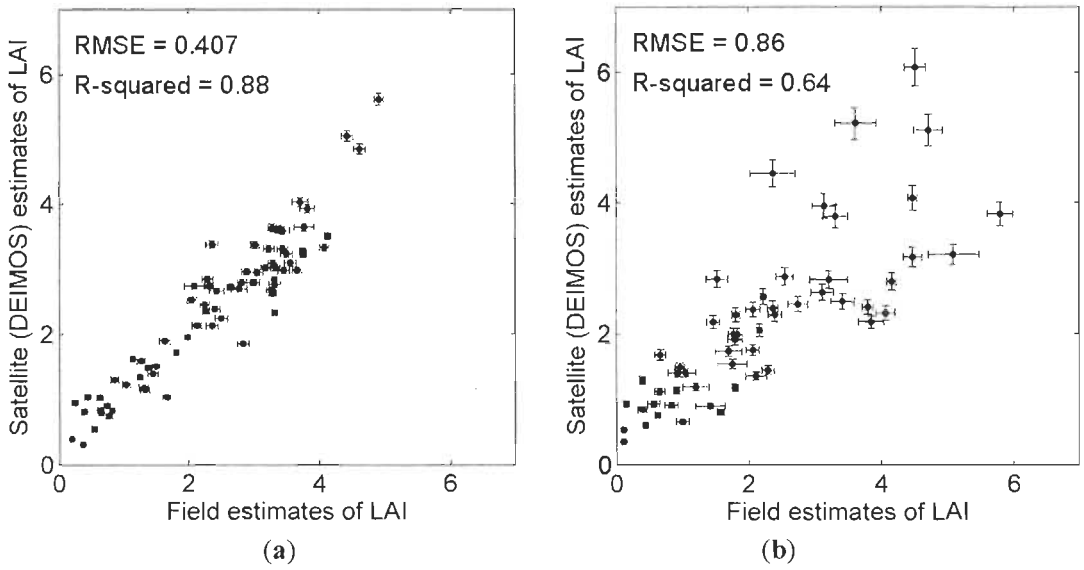

3.3. Transferability of LAI Estimation Models from One Test Site to Another

To test the transferability of the CLAIR model parameters from one test site to another we used the results obtained from the procedure 3 (see Table 1) based on image-specific soil line slope and $WDVI_\infty$, seasonal- and test site-specific α coefficients. An example of the LAI time-series maps derived with this procedure is presented in Figure 6.

Figure 6. An example of the LAI time-series of DEIMOS-1 satellite sensor data for an area in the Marchfeld region (Austria). The maps were derived using the CLAIR model with an image-specific tuning of the soil line slope and $WDVI_\infty$ and a constant α coefficient value.

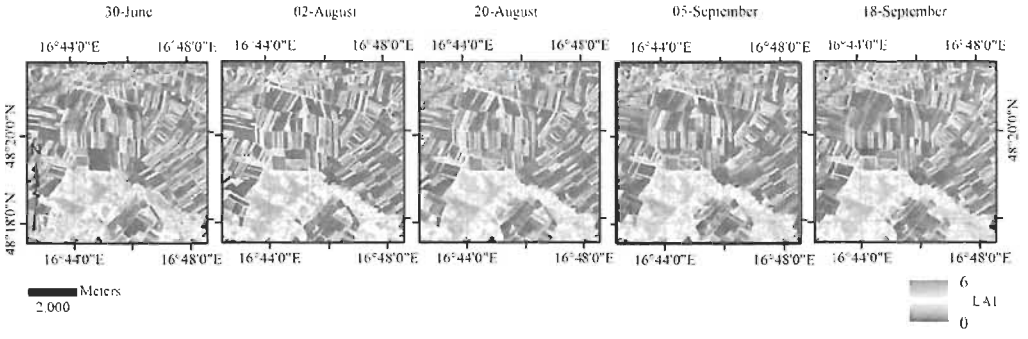

The reciprocal exchange of the calibrated models resulted in a RMSE of 0.412 and R^2 of 0.88 for the Italian test site. The RMSE for the Austrian test site was 0.855 with R^2 of 0.64. Both datasets responded a slight LAI underestimation starting from measured LAI values of 2.3 and higher. Percentage variations in the RMSE compared to test site specific models were lower than 0.5%.

Similarly, we tested the transferability of the SVM and RF regressions between test sites. The application of RF models provided a RMSE of 0.747 when transferring to Italian case study and a RMSE of 0.906 for the Austrian case study. In this case, we observed poorer prediction power compared to test site specific models, with a percentage increase in the RMSE up to 24.5%.

The mutual application of the SVM regression models provided a RMSE of 0.783 and of 0.808 for the Italian and Austrian case study respectively, with a percentage increase of the RMSE up 38.9% compared to test site specific models. A summary of the results is provided in Table 5.

Table 5. Transferability between test sites (IT: Italy; AT: Austria) of the CLAIR model, Random Forest and Support Vector Machine regressions. The parameters of the CLAIR model used in this comparison were derived following the procedure 3.

LAI Estimation Methods	Transferability	RMSE	R^2	Variations in RMSE (%) Compared to Test Site Specific Models
CLAIR model	IT with AT model	0.412	0.88	**+0.2%**
	AT with IT model	0.855	0.64	**−0.5%**
Random Forest	IT with AT model	0.747	0.75	+24.5%
	AT with IT model	0.906	0.61	+4.6%
Support Vector Machine	IT with AT model	0.783	0.79	+38.9%
	AT with IT model	0.808	0.69	+2.3%

4. Conclusions

In this study, we described a methodology to derive consistent time-series of Leaf Area Index (LAI) maps using an exponential relationship (CLAIR model) between LAI and the soil-line based Weighted Difference Vegetation Index (WDVI). The study analyzed different procedures for estimating the CLAIR model parameters (soil line slope, $WDVI_\infty$ and α coefficient) and highlighted the operational aspects of these approaches. We tested a seasonal average (constant) and an image-specific tuning to increase the consistency in the analysis of atmospherically corrected time-series images. Additionally, we applied two other statistical methods based on Random Forest (RF) and Support Vector Machine (SVM) regressions. These two algorithms, applied in several remote sensing problems have proved particularly useful in recent years for land cover classification. However, few studies can be found in the remote sensing literature for their application to biophysical parameter prediction problems.

The experimental analysis was conducted using a set of DEIMOS-1 satellite sensor data acquired over two agricultural regions in Southern Italy and Eastern Austria. In particular, these data were acquired in the context of two satellite-based irrigation advisory services; LAI maps are used as input in agro-meteorological models to derive crop water needs. This information is delivered directly to the farmers for water management purposes in nearly real time. The Italian case study represents already an operational service, while the Austrian site is a test-bed for further development and testing transferability of models and procedures from different environments, agricultural and management practices. Although limited to one satellite type only, this dataset offered the possibility to evaluate the transferability of the model parameters from one test site to another. This is particularly relevant in case no field measurements are available.

Using the CLAIR model with an image-specific tuning of the soil line slope and $WDVI_\infty$ and a constant α coefficient value provided the most accurate and consistent results (RMSE = 0.407 and 0.86 for Italy and Austria respectively). Notably, this approach has the minimum requirements for fieldwork. Considering this procedure, we also evaluated the transferability of the local model parameters between the two test sites observing a decrease in estimation accuracies smaller than 0.5%. RF and SVM regressions provided comparable results for each test site. However, we observed severe limitations in the transferability of these statistical methods between test sites with an increase in RMSE up to 24.5% for RF and 38.9% for SVM.

This work indicates that the CLAIR model can provide satisfactory accuracy if an adequate model parameterization is performed; results achieved here (with a limited number of spectral inputs) do not justify the use of advanced regression techniques (such as RF and SVM) compared to simple and robust semi-empirical relationships. One advantage of the semi-empirical model used in this study is that its parameters have a physical denotation and it is possible to interpret and explain the model behavior. In addition, it has the advantage of not requiring *a priori* crop map information. This additional layer could be used, if available, to perform a crop specific calibration of the extinction and scattering coefficient (α). However, this would require additional fieldwork to achieve a statistically significant number of measurements for each crop type.

Acknowledgements

The study was supported by the Austrian Space Application Programme (ASAP) in the context of the project 'EO4Water—Application of Earth observation technologies for rural water management' (www.eo4water.com) and by the 'Irrigation Advisory Services' of Campania Region, Italy (www.irrisat.it).

References

1. Lee, W.S.; Alchanatis, V.; Yang, C.; Hirafuji, M.; Moshou, D.; Li, C. Sensing technologies for precision specialty crop production. *Comput. Electron. Agric.* **2010**, *74*, 2–33.
2. NEREUS. *The Growing Use of GMES across Europe's Regions*; NEREUS: Bruxelle, 2012.
3. Bréda, N.J.J. Ground-based measurements of leaf area index: A review of methods, instruments and current controversies. *J. Exp. Bot.* **2003**, *54*, 2403–2417.
4. D'Urso, G.; Richter, K.; Calera, A.; Osann, M. A.; Escadafal, R.; Garatuza-Pajan, J.; Hanich, L.; Perdigão, A.; Tapia, J.B.; Vuolo, F. Earth Observation products for operational irrigation management in the context of the PLEIADeS project. *Agric. Water Manage.* **2010**, *98*, 271–282.
5. Jégo, G.; Pattey, E.; Liu, J. Using Leaf Area Index, retrieved from optical imagery, in the STICS crop model for predicting yield and biomass of field crops. *Field Crops Res.* **2012**, *131*, 63–74.
6. Casa, R.; Varella, H.; Buis, S.; Guérif, M.; De Solan, B.; Baret, F. Forcing a wheat crop model with LAI data to access agronomic variables: Evaluation of the impact of model and LAI uncertainties and comparison with an empirical approach. *Eur. J. Agron.* **2012**, *37*, 1–10.
7. Rembold, F.; Atzberger, C.; Rojas, O.; Savin, I. Using low resolution satellite imagey for yield prediction and yield anomaly detection. *Remote Sens.* **2013**, under review.

8. Doraiswamy, P.C.; Sinclair, T.R.; Hollinger, S.; Akhmedov, B.; Stern, A.; Prueger, J. Application of MODIS derived parameters for regional crop yield assessment. *Remote Sens. Environ.* **2005**, *97*, 192–202.
9. Ma, G.; Huang, J.; Wu, W.; Fan, J.; Zou, J.; Wu, S. Assimilation of MODIS-LAI into the WOFOST model for forecasting regional winter wheat yield. *Math. Comput. Model.* **2011**, in press.
10. Atzberger, C. Advances in remote sensing of agriculture: Context description, existing operational monitoring systems and major information needs. *Remote Sens.* **2013**, *5*, 949–981.
11. Baret, F.; Buis, S. Estimating Canopy Characteristics from Remote Sensing Observations: Review of Methods and Associated Problems. In *Advances in Land Remote Sensing*; Liang, S., Ed.; Springer: New York, NY, USA, 2008; pp. 173–201.
12. Dorigo, W.A.; Zurita-Milla, R.; De Wit, A.J.W.; Brazile, J.; Singh, R.; Schaepman, M.E. A review on reflective remote sensing and data assimilation techniques for enhanced agroecosystem modeling. *Int. J. Appl. Earth Obs. Geoinf.* **2007**, *9*, 165–193.
13. Atzberger, C.; Guérif, M.; Baret, F.; Werner, W. Comparative analysis of three chemometric techniques for the spectroradiometric assessment of canopy chlorophyll content in winter wheat. *Comput. Electron. Agric.* **2010**, *73*, 165–173.
14. Cho, M.A.; Skidmore, A.K.; Atzberger, C. Towards red edge positions less sensitive to canopy biophysical parameters for leaf chlorophyll estimation using properties optique spectrales des feuilles (PROSPECT) and scattering by arbitrarily inclined leaves (SAILH) simulated data. *Int. J. Remote Sens.* **2008**, *29*, 2241–2255.
15. Darvishzadeh, R.; Atzberger, C.; Skidmore, A.K.; Abkar, A.A. Leaf Area Index derivation from hyperspectral vegetation indicesand the red edge position. *Int. J. Remote Sens.* **2009**, *30*, 6199–6218.
16. Chen, J.M.; Pavlic, G.; Brown, L.; Cihlar, J.; Leblanc, S.G.; White, H.P.; Hall, R.J.; Peddle, D.R.; King, D.J.; Trofymow, J.A.; *et al.* Derivation and validation of Canada-wide coarse-resolution leaf area index maps using high-resolution satellite imagery and ground measurements. *Remote Sens. Environ.* **2002**, *80*, 165–184.
17. Wang, Y.J.; Woodcock, C.E.; Buermann, W.; Stenberg, P.; Voipio, P.; Smolander, H.; Hame, T.; Tian, Y.H.; Hu, J.N.; Knyazikhin, Y.; Myneni, R.B. Evaluation of the MODIS LAI algorithm at a coniferous forest site in Finland. *Remote Sens. Environ.* **2004**, *91*, 114–127.
18. Liu, J.; Pattey, E.; Jégo, G. Assessment of vegetation indices for regional crop green LAI estimation from Landsat images over multiple growing seasons. *Remote Sens. Environ.* **2012**, *123*, 347–358.
19. Hadjimitsis, D.G.; Clayton, C.R.I.; Retalis, A. The use of selected pseudo-invariant targets for the application of atmospheric correction in multi-temporal studies using satellite remotely sensed imagery. *Int. J. Appl. Earth Obs. Geoinf.* **2009**, *11*, 192–200.
20. Richter, R. Correction of satellite imagery over mountainous terrain. *Appl. Opt.* **1998**, *37*, 4004–4015.
21. Liang, S.; Member, S.; Fang, H.; Chen, M. Atmospheric correction of Landsat ETM+ land surface imagery. I. Methods. **2001**, *39*, 2490–2498.

22. Laurent, V.C.E.; Verhoef, W.; Clevers, J.G.P.W.; Schaepman, M.E. Estimating forest variables from top-of-atmosphere radiance satellite measurements using coupled radiative transfer models. *Remote Sens. Environ.* **2011**, *115*, 1043–1052.
23. Baret, F.; Guyot, G. Potentials and limits of vegetation indices for LAI and APAR assessment. *Remote Sens. Environ.* **1991**, *35*, 161–173.
24. Clevers, J.G.P.W. Application of a weighted infrared-red vegetation index for estimating leaf Area Index by Correcting for Soil Moisture. *Remote Sens. Environ.* **1989**, *29*, 25–37.
25. Clevers, J.G.P.W.; Vonder, O.W.; Jongschaap, R.E.E.; Desprats, J.F.; King, C.; Prévot, L.; Bruguier, N. A semi-empirical approach for estimating plant parameters within the RESEDA-project. *Int. Arch. Photogramm. Remote Sens. Spat. Inform. Sci.* **2000**, *XXXIII*, 272–279.
26. Vuolo, F.; Atzberger, C.; Richter, K.; D'Urso, G.; Dash, J. Retrieval of Biophysical Vegetation Products from RapidEye Imagery. In *ISPRS TC VII Symposium—100 Years ISPRS*; Wagner, W.; Szekely, B., Eds.; ISPRS: Vienna, Austria; 2010; Vol. XXXVIII, pp. 281–286.
27. Capodici, F.; D'Urso, G.; Maltese, A. Investigating the relationship between X-band SAR data from COSMOS-Skymed satellite and NDVI for LAI detection. *Remote Sens.* **2012**, under review.
28. Clevers, J.G.P.W. The derivation of a simplified reflectance model for the estimation of leaf area index. *Remote Sens. Environ.* **1988**, *25*, 53–69.
29. De Michele, C.; Vuolo, F.; D'Urso, G.; Marotta, L.; Richter, K. The Irrigation Advisory Program of Campania Region: From research to operational support for the Water Directive in Agriculture. In Proceedings of 33rd International Symposium on Remote Sensing of Environment (ISRSE), Stresa, Italy, 4–8 May 2009.
30. Bonfante, A.; Alfieri, M.; Basile, A.; De Lorenzi, F.; Fiorentino, N.; Menenti, M. The Evaluation of the Climate Change Effects on Maize and Fennel Cultivation by Means of an Hydrological Physically Based Model: The Case Study of an Irrigated District. In Proceedings of EGU General Assembly 2012, Vienna, Austria, 22–27 April 2012; p.7807.
31. Coppola, E.; Capra, G.F.; Odierna, P.; Vacca, S.; Buondonno, A. Lead distribution as related to pedological features of soils in the Volturno River low Basin (Campania, Italy). *Geoderma* **2010**, *159*, 342–349.
32. Sequino, V.; Zucaro, R.; D'Alterio, D.; Valente, M.; Frunzio, M.; Iavarone, V.; Belmare, E.; Serpico, G. *Stato dell'irrigazione in Campania*; 1999; p. 109.
33. Richter, K.; Rischbeck, P.; Eitzinger, J.; Schneider, W.; Suppan, F.; Weihs, P. Plant growth monitoring and potential drought risk assessment by means of Earth observation data. *Int. J. Remote Sens.* **2008**, *29*, 4943–4960.
34. LI-COR. *LAI-2000 Plant Canopy Analyzer Instruction Manual Lincoln*; LI-COR Inc.: Lincoln, NE, USA, 1992.
35. Leblanc, S.G.; Chen, J.M. A practical scheme for correcting multiple scattering effects on optical LAI measurements. *Agric. Forest Meteorol.* **2001**, *110*, 125–139.
36. Welles, I.J.; Norman, J.M. Instrument for indirect measurement of canopy architecture. *Agron. J.* **1991**, *83*, 818–825.
37. Garriques, S.; Shabanov, N.V; Swanson, K.; Morisette, J.T.; Baret, F.; Myneni, R.B. Intercomparison and sensitivity analysis of Leaf Area Index retrievals from LAI-2000, AccuPAR, and digital hemispherical photography over croplands. *Agric. Forest Meteorol.* **2008**, *148*, 1193–1209.

38. Baret, F.; Jacquemoud, S.; Hanocq, J.F. The soil line concept in remote sensing. *Remote Sens. Rev.* **1993**, *7*, 65–82.
39. Steyerberg, E.W.; Harrell, F.E.; Borsboom, G.J.; Eijkemans, M.J.; Vergouwe, Y.; Habbema, J.D. Internal validation of predictive models: Efficiency of some procedures for logistic regression analysis. *J. Clin. Epidemiol.* **2001**, *54*, 774–81.
40. Richter, K.; Atzberger, C.; Hank, T.B.; Mauser, W. Derivation of biophysical variables from Earth observation data: Validation and statistical measures. *J. Appl. Remote Sens.* **2012**, *6*, 063557.
41. Vapnik, V. *The Nature of Statistical Learning Theory*; Springer-Verlag: New York, NY, USA, 1995.
42. Vapnik, V.; Golowich, S.E.; Smola, A.J. Support Vector Method for Function Approximation, Regression Estimation and Signal Processing. In *Advances in Neural Information Processing Systems 9—Proceedings of the 1996 Neural Information Processing Systems Conference (NIPS 1996)*; Mozer, M.; Jordan, M. I.; Petsche, T., Eds.; MIT Press: Cambridge, MA, USA, 1997; pp. 281–287.
43. Yang, X.; Huang, J.; Wu, Y.; Wang, J.; Wang, P.; Wang, X.; Huete, A.R. Estimating biophysical parameters of rice with remote sensing data using support vector machines. *Sci. China. Life Sci.* **2011**, *54*, 272–81.
44. Wang, F.; Huang, J.; Lou, Z. A comparison of three methods for estimating leaf area index of paddy rice from optimal hyperspectral bands. *Precis. Agr.* **2011**, *12*, 439–447.
45. Camps-Valls, G.; Munoz-Mari, J.; Gomez-Chova, L.; Richter, K.; Calpe-Maravilla, J. Biophysical parameter estimation with a semisupervised Support Vector Machine. *IEEE Geosci. Remote Sens. Lett.* **2009**, *6*, 248–252.
46. Verrelst, J.; Muñoz, J.; Alonso, L.; Delegido, J.; Rivera, J.P.; Camps-Valls, G.; Moreno, J. Machine learning regression algorithms for biophysical parameter retrieval: Opportunities for Sentinel-2 and -3. *Remote Sens. Environ.* **2012**, *118*, 127–139.
47. Smola, A.; Schölkopf, B. A tutorial on support vector regression. *Statist. Comput.* **2004**, *14*, 199–222.
48. Suykens, J.A.K.; Van Gestel, T.; De Brabanter, J.; De Moor, B.; Vandewalle, J. *Least Squares Support Vector Machines*; World Scientific Pub.Co.: Singapore, 2002.
49. Breiman, L. Random Forests. *Mach. Learn.* **2001**, *45*, 5–32.
50. Powell, S.L.; Cohen, W.B.; Healey, S.P.; Kennedy, R.E.; Moisen, G.G.; Pierce, K.B.; Ohmann, J.L. Quantification of live aboveground forest biomass dynamics with Landsat time-series and field inventory data: A comparison of empirical modeling approaches. *Remote Sens. Environ.* **2010**, *114*, 1053–1068.
51. Le Maire, G.; Marsden, C.; Nouvellon, Y.; Grinand, C.; Hakamada, R.; Stape, J.-L.; Laclau, J.-P. MODIS NDVI time-series allow the monitoring of Eucalyptus plantation biomass. *Remote Sens. Environ.* **2011**, *115*, 2613–2625.
52. Liaw, A.; Wiener, M. Classification and regression by randomForest. *R News* **2002**, *2*, 18–22.

Bibliography

[1] Http://iwhw.boku.ac.at/LVA816302/downloadpdf.html, "Hydrologie Österreichs - Marchfeld."

[2] T. Dillehay, H. Eling, and J. Rossen, "Preceramic irrigation canals in the Peruvian Andes.," *Proceedings of the National Academy of Sciences of the United States of America*, vol. 102, pp. 17241–4, Nov. 2005.

[3] J. Foley, N. Ramankutty, K. Brauman, E. Cassidy, J. Gerber, M. Johnston, N. Mueller, C. O'Connell, D. Ray, P. West, C. Balzer, E. Bennett, S. Carpenter, J. Hill, C. Monfreda, S. Polasky, J. Rockström, J. Sheehan, S. Siebert, D. Tilman, and D. Zaks, "Solutions for a cultivated planet.," *Nature*, vol. 478, pp. 337–42, Oct. 2011.

[4] N. Mueller, J. Gerber, M. Johnston, D. Ray, N. Ramankutty, and J. Foley, "Closing yield gaps through nutrient and water management.," *Nature*, vol. 490, pp. 254–7, Oct. 2012.

[5] D. Tilman, C. Balzer, J. Hill, and B. L. Befort, "Global food demand and the sustainable intensification of agriculture.." *Proceedings of the National Academy of Sciences of the United States of America*, vol. 108, pp. 20260–4, Dec. 2011.

[6] D. Seckler, U. Amarasinghe, D. Molden, R. de Silva, and R. Barker, "World Water Demand and Supply, 1990 to 2025: Scenarios and Issues," *International Water Management Institute*, p. 40 pp., 1999.

[7] R. Collins, P. Kristensen, and N. Thyssen, "Water resources across Europe-confronting water scarcity and drought," no. 2, 2009.

[8] J. W. Alan Buis, Steve Cole, "NASA Satellites Find Freshwater Losses in Middle East," 2013.

[9] N. C. K. Kenneth K. Tanji, *Agricultural drainage water management in arid and semi-arid areas*. Food and Agriculture Organization of the United Nations, 2002.

[10] M. Trnka, J. Eitzinger, M. Dubrovsky, D. Semerádová, P. Štepánek, P. Hlavinka, J. Balek, P. Skalák, A. Farda, H. Formayer, and Z. Žalud, "Is rainfed crop production in central Europe at risk? Using a regional climate model to produce high resolution agroclimatic information for decision makers," *The Journal of Agricultural Science*, vol. 148, no. 06, pp. 639 656.

[11] M. Trnka, M. Dubrovský, M. Svoboda, D. Semerádová, M. Hayes, Z. Zalud, and D. Wilhite, "Developing a regional drought climatology for the Czech Republic," *International Journal of Climatology*, vol. 29, pp. 863–883, May 2009.

[12] J. S. Pal, "Consistency of recent European summer precipitation trends and extremes with future regional climate projections," *Geophysical Research Letters*, vol. 31, no. 13, p. L13202, 2004.

[13] M. Dubrovsky, M. D. Svoboda, M. Trnka, M. J. Hayes, D. A. Wilhite, Z. Zalud, and P. Hlavinka, "Application of relative drought indices in assessing climate-change impacts on drought conditions in Czechia," *Theoretical and Applied Climatology*, vol. 96, pp. 155–171, Apr. 2008.

[14] J. Eitzinger, K. Kersebaum, and H. Formayer, *Landwirtschaft im Klimawandel: Auswirkungen und Anpassungsstrategien für die land- und forstwirtschaftlichen Betriebe in Mitteleuropa [Broschiert]*. Agrimedia, 2009.

[15] R. M. S. e. Meredith A. Giordano, Frank R. Rijsberman, *"More Crop Per Drop": Revisiting a Research Paradigm: Results and Synthesis of Iwmi's Research 1996-2005*. IWA Publishing, 2006.

[16] D. Luquet, A. Vidal, M. Smith, J. Dauzat, and V. A. Luquet D., "More crop per drop: how to make it acceptable for farmers?," 2005.

[17] R. Colwell, *Determining the Prevalence of certain Cereal Crop Diseases by means of Aerial Photography*. Berkeley: Berkeley, 1956.

[18] H. G. Jones and R. A. Vaughan, *Remote Sensing of Vegetation: Principles, Techniques, and Applications*. Oxford University Press, USA, 2010.

[19] N. J. J. Bréda, "Ground-based measurements of leaf area index: a review of methods, instruments and current controversies.," *Journal of experimental botany*, vol. 54, pp. 2403–17, Nov. 2003.

[20] G. D'Urso, F. Vuolo, K. Richter, A. Calera Belmonte, and M. A. Osann, "Earth observation products for operational irrigation management: the PLEIADeS project," in *SPIE Europe Remote Sensing* (C. M. U. Neale and A. Maltese, eds.), pp. 74720D–74720D–11, Sept. 2009.

[21] G. Jégo, E. Pattey, and J. Liu, "Using Leaf Area Index, retrieved from optical imagery, in the STICS crop model for predicting yield and biomass of field crops," *Field Crops Research*, vol. 131, pp. 63–74, May 2012.

[22] R. Casa, H. Varella, S. Buis, M. Guérif, B. De Solan, and F. Baret, "Forcing a wheat crop model with LAI data to access agronomic variables: Evaluation of the impact of model and LAI uncertainties and comparison with an empirical approach," *European Journal of Agronomy*, vol. 37, pp. 1–10, Feb. 2012.

[23] F. Rembold, C. Atzberger, I. Savin, and O. Rojas, "Using Low Resolution Satellite Imagery for Yield Prediction and Yield Anomaly Detection," *Remote Sensing*, vol. 5, pp. 1704–1733, Apr. 2013.

[24] P. C. Doraiswamy, T. R. Sinclair, S. Hollinger, B. Akhmedov, A. Stern, and J. Prueger, "Application of MODIS derived parameters for regional crop yield assessment," *Remote Sensing of Environment*, vol. 97, pp. 192–202, July 2005.

[25] G. Ma, J. Huang, W. Wu, J. Fan, J. Zou, and S. Wu, "Assimilation of MODIS-LAI into the WOFOST model for forecasting regional winter wheat yield," *Mathematical and Computer Modelling*, vol. null, Nov. 2011.

[26] C. Atzberger, "Advances in Remote Sensing of Agriculture: Context Description, Existing Operational Monitoring Systems and Major Information Needs," *Remote Sensing*, vol. 5, pp. 949–981, Feb. 2013.

[27] G. Schultz, *Remote Sensing in Hydrology and Water Management*. Springer, 2000.

[28] G. D'Urso, *On-demand irrigation systems : A combined agrohydrological and remote sensing approach*. PhD thesis, Wageningen University, 2001.

[29] J. Clevers, "Application of a weighted infrared-red vegetation index for estimating leaf Area Index by Correcting for Soil Moisture," *Remote Sensing of Environment*, vol. 29, pp. 25 37, 1989.

[30] Commission of the European Communities, "CORINE Land Cover," 1995.

[31] W. Neudorfer, *Wasserschutz und Lebensader Marchfeldkanal*. Marchfeld Kanal, 2002.

[32] K. Richter, P. Rischbeck, J. Eitzinger, W. Schneider, F. Suppan, and P. Weihs, "Plant growth monitoring and potential drought risk assessment by means of Earth observation data," *International Journal of Remote Sensing*, vol. 29, pp. 4943- 4960, Sept. 2008.

[33] Http://www.bmvit.gv.at/verkehr/schifffahrt/wasserstrassen/wasserbau.html, "Wasserbau im Marchfeld."

[34] W. Neudorfer, "personal communication," 2013.

[35] R. Allen, L. Pereira, D. Raes, M. Smith, W. Ab, D. Raes, and M. Smith, *Crop evapotranspiration - Guidlines for computing crop water requirements*. Food and Agriculture Organization of the United Nations, 1998.

[36] D. W. Eckhardt, J. P. Verdin, and G. R. Lyford, "Automated update of an irrigated lands GIS using SPOT HRV imagery," *Photogrammetric Engineering & Remote Sensing*, vol. 56, no. 11, pp. 1515–1522, 1990.

[37] D. G. Hadjimitsis, C. R. I. Clayton, and A. Retalis, "The use of selected pseudo-invariant targets for the application of atmospheric correction in multi-temporal studies using satellite remotely sensed imagery," *International Journal of Applied Earth Observation and Geoinformation*, vol. 11, no. 3, pp. 192–200, 2009.

[38] F. Baret, S. Jacquemoud, and J. F. Hanocq, "About the soil line concept in remote sensing," vol. 13, no. 5, pp. 281–284, 1993.

[39] A. DUrso, G., Calera Belmonte, "Operative Approaches To Determine Crop Water Requirements From Earth Observation Data: Methodologies And Applications," in *AIP Conference Proceedings*, vol. 852, pp. 14–25, AIP, Aug. 2006.

[40] F. Vuolo, N. Neugebauer, S. Bolognesi, C. Atzberger, and G. D'Urso, "Estimation of Leaf Area Index Using DEIMOS-1 Data: Application and Transferability of a Semi-Empirical Relationship between two Agricultural Areas," *Remote Sensing*, vol. 5, pp. 1274–1291, Mar. 2013.

[41] Www.marchfeldkanal.at/09main13h.htm, "Daten, Fakten, Zahlen."